

Spreading of Baltic Deep Water: A Case Study for the Winter 1997-1998

Eberhard Hagen and Rainer Feistel

Summary

Exceptionally saline water with the mean volume flux of about $10 \text{ km}^3/\text{d}$ passed the Danish straits during the winter 1997-98 to spread towards the Baltic Proper. The released inflow event is discussed by means of different hydrographic data sets. For the first time, its influence on the deep circulation of the Eastern Gotland Basin was continuously documented. Time series of temperature and current with a length of more than one year precisely determined the duration of that inflow. It started over the eastern topographic flank of this basin and lasted 130 days. Once in the basin, the spreading of dense deep water formed a wedge-shaped frontal zone rotating anticlockwise with the background velocity of about 3 cm/s . Beneath 170 m depth, associated currents roughly followed the isobaths. Adjacent intrusions intensified this cyclonic deep water rotation by a factor of two while rhythmically occurring inflow pulses with a quasi-period of about 20 days additionally accelerated the circulation by a factor of about three. A total of six pulses induced a high temporal variability in mass and current fields. They were accompanied by linearly increasing temperatures within near bottom layers. Each new inflow pulse started on the thermal level of previous pulses. Finally, the net intrusion of warm, saline, but weakly oxygenated dense water completely fulfilled the closed basin volume of 38 km^3 . The associated mean volume flux was about $0.3 \text{ km}^3/\text{d}$. Released upward motions well integrated vertical changes of the topographic volume. This follows from the comparison of two eddy resolving data sets, which were obtained from hydrographic surveys carried out during the pre-inflow and post-inflow situation.

1. Introduction

Spatial and temporal variations in both the mass and current field cover a large range of spatial and temporal scales and characterise the circulation in the relatively shallow Baltic Sea, DIETRICH (1950). River run-offs provide a supply of fresh water of about $470 \text{ km}^3/\text{y}$ with monthly peak values of about 60 km^3 in May/ June, cf. BROGMUS (1952) and HELCOM (1986). Therefore, a low-density surface layer permanently exists in the whole Baltic Sea. Its salinity content varies between 7 and 8 psu. Comparing mean sea levels of the Kattegat, which is part of the transition zone between the North Sea and the Baltic Sea, with those of the Baltic Proper it reveals that the related surplus of brackish surface water is responsible for positive anomalies in the central Baltic and negative anomalies in the Kattegat. The resulting incline of the sea surface causes the outflow of low saline water in near-surface layers. Under the influence of the deflecting Coriolis force it mainly spreads through the Belt Sea towards the Kattegat to feed the Baltic Current, which follows Swedish and Norwegian coasts into the North Sea. Geographical notations are depicted in Fig. 1.

Depending on highly variable forcing fields, as they are given by winds and adjacent sea level anomalies, salty water of the Kattegat flows through the Danish Belts and the Sound to compensate the mentioned outflow. Associated events sporadically overflow several shallow sills on their way towards the first Baltic basin, the Arkona Basin. Here, dense bottom water is formed to be intermediately stored for a certain time in a 'bottom pool', STIGEBRANDT and WULFF (1987). During that stay time, entrainment adds about 50% of intermediate water to the deep water, KOUTS and OMSTEDT (1993). Its farther eastward penetration is accompanied by dilution processes acting vertically. Properties of upper layer water are mixed downward and mixing also 'lifts' thermohaline properties of near bottom water into intermediate layers, cf. WALIN (1981) and STIGEBRANDT (1985). Thermohaline water properties in the upper layer of dense bottom currents are transformed permanently. The deep water becomes less dense and is,

more or less, neutrally buoyant. The resulting mixed water types spread at different pressure levels along the line of steepest descend in the water depth from basin to basin. Hydrographic standard stations of the Baltic Monitoring Programme (BMP) follow this line in Fig.1.

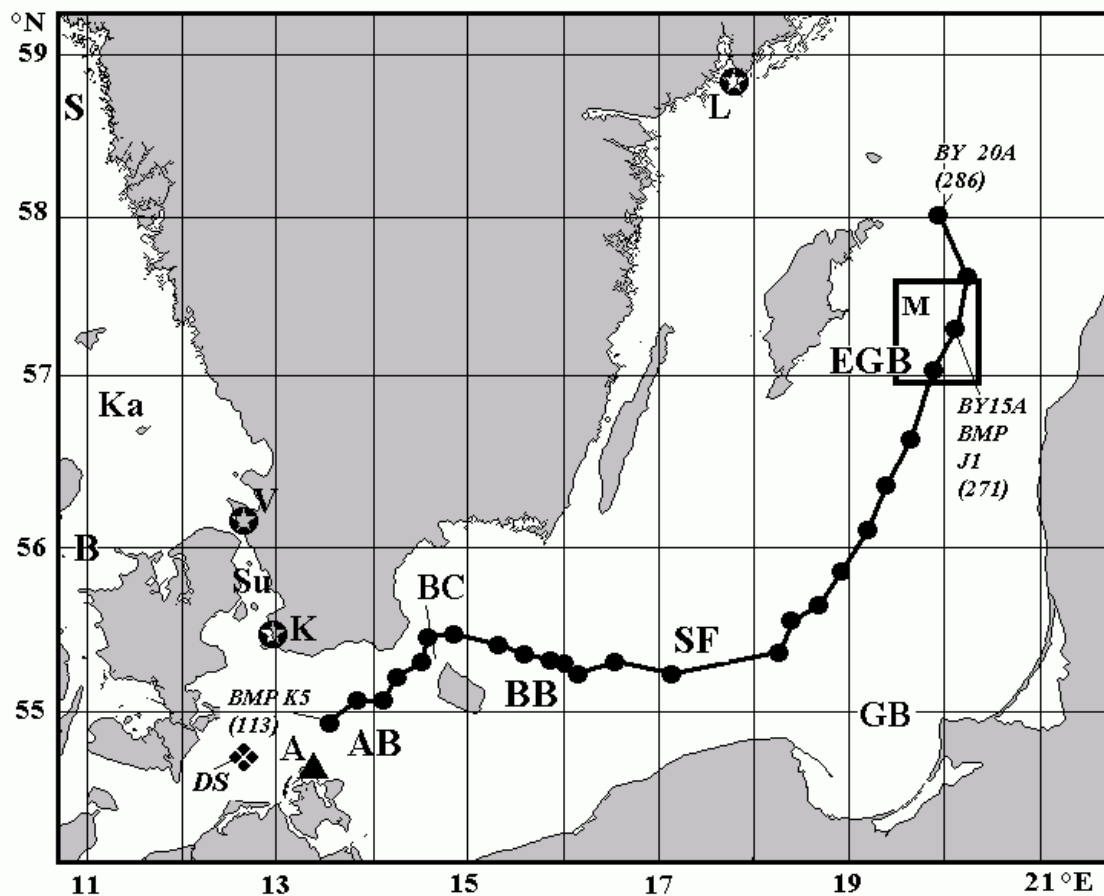


Fig.1 Geographical notations in the Baltic Sea with a transect composed by selected stations (dots) of the Baltic Monitoring Programme; this section starts with station 113 in the south-west and ends with station 286 in the north-east; the position of the Darss Sill station and that of the station Arkona are shown as well as Swedish sea level stations (stars); the area of the MESODYN (M) project involves the central BMP station 271 in the Eastern Gotland Basin:

- S = Skagerrak
- Ka = Kattegat
- V = Sea level station 'Viken'
- B = Belts
- Su = Sound
- K = Sea level station 'Klagshamn'
- DS = Darss Sill station
- A = Meteorological station 'Arkona'
- AB = Arkona Basin
- BC = Bornholm Channel
- BB = Bornholm Basin
- SF = Stolpe Furrow
- GB = Gdansk Basin

EGB = Eastern Gotland Basin
L = Sea level station 'Landsort'

From the Arkona Basin via Bornholm's Channel with a sill depth of about 48 m, cf. LARSEN and KÖGLER (1975), the main path-way of deep currents continues into the Bornholm Basin. Here, the modification of dense near bottom water reduces the salinity. There is some observational evidence that much of the diapycnal mixing is actually done before the dense deep water is incorporated into the deep water of the Baltic Proper. Generally, surface and deep waters are separated by a pronounced pycnocline consisting of a permanent halocline in depths between 35 m and 40 m in the Arkona Basin but between 65 m and 75 m depth in the EGB. This main pycnocline (halocline) can be monitored in the whole Baltic Sea. In addition, a significant thermocline develops at depths between 10 m and 30 m during summer environmental conditions, MATTHÄUS (1984). It vanishes during the following winter due to released convection processes, which are caused by wintry cooling at the sea surface. However, dynamics of near surface and intermediate layers are essentially separated from those of deep layers by the main pycnocline. Consequently, deep layers of each Baltic basin reveal characteristic thermohaline properties, which are discussed in more detail by OMSTEDT and AXELL (1998).

Inflow events influence water properties of all Baltic basins when the density of the resulting mixed water of the previous basin exceeds the density of old deep water of the following basin. Under such preconditions, dense deep water propagates from the Bornholm Basin via the Stolpe Furrow towards both the Gdansk Basin and the Eastern Gotland Basin (EGB). Otherwise 'stagnant conditions' characterise the hydrography of deepest layers for several years. That means an effective inflow event provides a sufficient volume flux of relatively high salinity which is able to fulfil all adjacent basins with extremely dense water. The reaction of the deep water in the EGB on such inflows was, for instance, described by KALLE (1943). Further studies by WYRTKI (1954), WOLF (1972), BÖRNGEN (1978), and SCHINKE and MATTHÄUS (1998) discussed several dynamics and necessary preconditions in meteorological forcing fields. It became evident that identified inflow events involve a characteristic repeating time between three and seven years. For instance, MATTHÄUS and FRANCK (1992) identified 90 of them between 1897 and 1976. They showed that the averaged duration of 'Major Baltic Inflows' fluctuates between 11 days and 29 days. On average, the Baltic sea level rises by about 0.3 m between the first day of the inflow and the day of maximum sea level anomaly. Subsequently, the changed volume of highly saline water is larger than 100 km³ during strong events. Each of such major inflow event is frequently preceded by an inflow of less saline water. Related aspects were investigated in more detail by LASS (1988), LASS and SCHWABE (1990), and LASS and MATTHÄUS (1996) while biological and chemical consequences were extensively discussed by NEHRING and FRANCKE (1981) for three inflow events, which occurred during the winters 1968/69, 1972, 1976/77. Here, we may summarise three necessary preconditions:

- easterly winds lasting for several weeks over the whole Baltic immediately followed by strong westerly winds of similar duration,
- lower than normal sea levels in the western Baltic Sea (Arkona Basin) and higher than normal sea levels in Skagerrak and Kattegat during the start of the inflow,
- positive anomalies in salinity of near bottom water in the Kattegat.

Furthermore, it seems to be that there are two different categories of inflow events with respect to their seasonal occurrence and associated hydrographic conditions:

- Late autumn - early winter type: eastward spreading of relatively warm but highly saline water with a relatively low content of dissolved oxygen with a duration between 15 days and 20 days.
- Late winter - early spring type: 20 days until 25 days lasting eastward spreading of relatively cold and saline water, which is comparatively well oxygenated.

Finally, 'Major Baltic Inflows' inject a total of about 300 km³ saline water and last about 32 days, MATTHÄUS and FRANCK (1992). During that relatively short time period, they are accompanied by an mean volume transport of about 9 km³/d.

Due to intense activities of the Baltic fishery during the whole year no long time series with the length of a complete seasonal cycle are available from drifters and/ or moored strings, which are equipped with current meters and thermosalinographs. However, such observations are necessary to describe the influence of such inflow events on deep compensation currents properly. The aim of this study is to present an observational example dealing with the inflow event of the winter 1997-1998. Current meters and recording thermometers, which were deployed beneath the perennial pycnocline at two positions in the EGB, provide such long time series. Resulting data sets were analysed in context with different hydrographic data to describe the response of the deep water circulation of the EGB on that inflow event in more detail. Finally, plausible working hypotheses of related dynamics are discussed.

2. Data Base

The climatic behaviour of temperature, salinity and dissolved oxygen was estimated by means of historical data, which are available from the Baltic Monitoring Programme (BMP) of the Institute for Baltic Sea Research Warnemuende (IOW). In order to describe climatic tendencies in the hydrographic regime of the deep mass field in the EGB, we used data of the central station no. 271 at 57°18.3'N, 20°04.6'E (BMP J1). Its position coincides with the former Baltic Year station BY15A and indicates the water depth of 242 m. Starting in 1969 until now, the BMP data set involves irregularly distributed measurements not only in time but also in depth. Samples of Nansen bottles and CTD profiles show gaps between some days up to several months around UNESCO-standard depths. Data of neighbouring horizons were linearly interpolated to reconstruct continuous time series for temperature, salinity, and dissolved oxygen at 170 m depth for comparison with actual records from thermometers and current meters. Equivalents of hydrogen sulfide have been expressed by negative values of oxygen according to NEHRING and FRANCKE (1981). Hydrographic data sets of three BMP cruises are additionally used to describe the hydrographic fields during October 1997, February 1998, and May 1998. Positions of selected stations are shown in Fig.1. Measurements regularly started in the south-west (Arkona Basin) and ended north of the EGB. The German Weather Service provided hourly values of both wind velocity and wind direction recorded at the station Arkona, which locates at the northern top of the Ruegen Island. Its position is shown by a triangle in Fig.1. Wind values were decomposed in their zonal ($U_w > 0$ to the east) and meridional components ($V_w > 0$ to the north). The Marine Monitoring Network (MARNET) of the Federal Maritime and Hydrographic Agency Hamburg (BSH) provided hourly data recorded continuously at the Darss Sill station (54° 42' N, 12° 42' E) from August 1997 until May 1998. Its position is named (DS) in Fig.1. Here, the water depth is 21 m. Seacat-16 recorder measured temperature and salinity by a sampling frequency of 10 minutes at horizons of 7 m, 12 m, 17 m, and 19.5 m. The achieved accuracy is about 0.01 K and 0.02 psu, respectively. A moored Acoustic Doppler Current Profiler (ADCP, 600 kHz) measured the motion field above the Darss Sill. Due to different recording gaps, time series of horizontal current components were selected from comparable horizons for a time interval of 14 days. Technical details of the station DS are discussed by KRÜGER (1997).

Hourly sea level data of stations 'Viken' (transition zone between the Kattegat and the entry of the Sound), 'Klagshamn' (entry of the Sound into the western Baltic Sea) and 'Landsort' (central Baltic Sea) were committed by the Swedish Meteorological and Hydrological Institute (SMHI) for the time between August 1997 and May 1998. Station positions are shown in Fig.1. Their reference level is determined by the Swedish Height System 1970 (RH70). Additionally, there were two hydrographic field campaigns with r/v 'A.v.Humboldt' to study meso-scale patterns in

the mass field of the deep EGB. Both surveys attribute to the IOW project 'Meso-scale Dynamics (MESODYN)' planned for five years (1996- 2000) in deep Baltic basins. The area under investigation is denoted by (M) in Fig.1. The data set of the first cruise (29 August- 4 September, 1997) excludes the influence of wintry convection processes while that of the second cruise (19 – 24 April, 1998) describes a late winter situation, which involves vertical convection due to cooling processes starting at the sea surface. The station map of the MESODYN project is shown in Fig.2. It covers the region between (56°55' -57°35') N and (19°32' - 20°28') E.

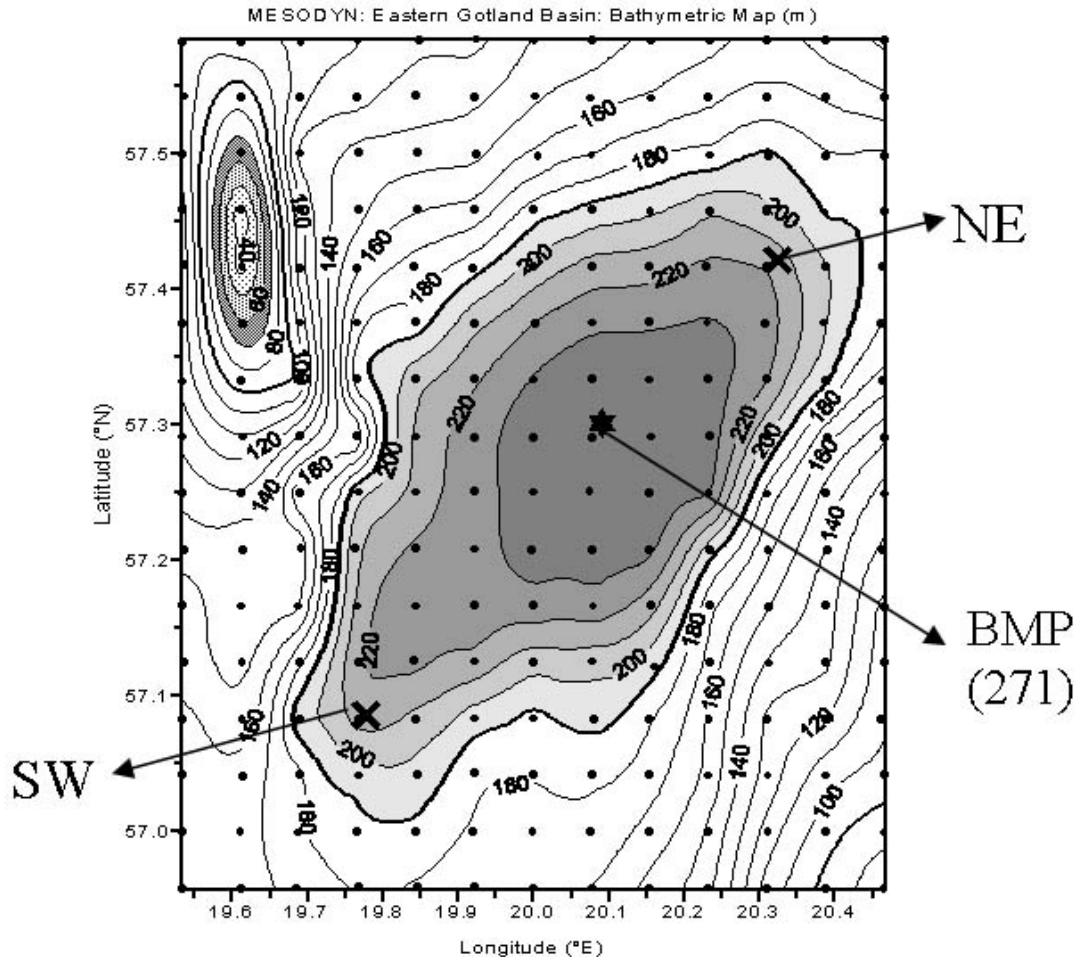


Fig.2 Area of investigation in the Eastern Gotland Basin with CTD-stations of the MESODYN- project (dots); crosses indicate positions of moored strings at the NE position and SW position; the position of the BMP station 271 (star) marks the centre of the basin; the bathymetric map (m) results from three echo sounded surveys with a station spacing of 2.5 n.m., its spatially and temporally averaged uncertainty is ± 0.27 m.

Conductivity (C), Salinity (S), temperature (T), pressure/ depth (D), and dissolved oxygen (O_2) have been profiled with a CTDO SeaBird probe from the sea surface down to near bottom layers. During both MESODYN field campaigns, a total of 2x208 CTDO stations (16 zonal sections x 13 stations) was spatially resolved by a regular station grid with a spacing of 2.5 n.m. (4.6 km). Measurements started in the north-west corner to follow zonal transects. In the central EGB, the first mode radius of deformation can be expected to be in the range between 7 km and 10 km, cf. FENNEL et al. (1991). We obtained the spatially averaged value of 9 km (September, 1997) and 7

km (April, 1998). Concerning the station resolution of about 4.5 km for both MESODYN surveys, crucial effects of aliasing should be excluded. The situation is much more unfavourable for data of the monitoring programme with a station spacing up to 70 km, cf. Fig. 1.

The sensor temperature was daily controlled by three reversing thermometers at different depths. The resulting rms error was ± 0.003 K without any statistical correlation with pressure. In the following we use ($^{\circ}$ C) for absolute temperatures but (K) for differences and derived quantities like standard deviation and variance. The reference level of the potential temperature (density) was always selected to be at the sea surface. The salinity of the CTD probe has been compared with salinometer measurements with the averaged rms of ± 0.0007 psu. Comparisons with Winkler's method provided the corresponding range of ± 0.49 ml/l for dissolved oxygen. Actual sound speeds of CTD profiles were used to calibrate the echo-sounder for proper bathymetric maps of all MESODYN surveys. The resulting topography of the EGB is mapped in Fig. 2 with relative uncertainties in the range of ± 0.27 m. Due to changes in sea level, the absolute error is expected to be ± 1 m. Concerning the depth contours of other deep Baltic basins of the MESODYN project we refer to REISSMANN (1999).

To study temporal variations in the mass and current field, two subsurface moorings were deployed at water depths of about 220 m in the south-west (SW: $57^{\circ}04.53'N$, $19^{\circ}45.12'E$) and in the north-east of the EGB (NE: $57^{\circ}25.38'N$, $20^{\circ}20.83'E$) on August 29, 1997 (positions NE and SW in Fig. 2.). The top of both moorings reached about 130 m depth. Each string was equipped with one recording current meters and thermometer (Aanderra RCM-7) at 170 m depth beneath the permanent pycnocline. The sampling interval of the RCM's was one hour. For a better vertical resolution of the thermal field, two thermometers (Hugrun- Seamon-Mini) additionally recorded the temperature at 140 m and 155 m depth at each string. Their data capacity is limited to 21000 values totally and allowed a sampling interval of 30 minutes. Both moorings have been recovered in July (NE-position) and in November (SW-position), 1998. Current velocity and current direction were decomposed into zonal (u = positive eastward) and meridional (v = positive northward) components. Thereafter, daily means and daily variances have been computed for all time series. Such procedure additionally provides the daily mean kinetic energy $MKE = (u^2 + v^2)/2$ per unit mass and via daily variances (σ^2) the related eddy kinetic energy $EKE = (\sigma_u^2 + \sigma_v^2)/2$. In a compact manner, the latter parameter illustrates the energetic level of current fluctuations shorter than the daily cycle.

3. Temporal Changes

Effective 'Major Inflows' are reported from the winter 1975/76 by NEHRING and FRANCKE (1981) and from the winter 1992/93 by MATTHÄUS and LASS (1995). The stagnant period in between both inflow events was accompanied by decreasing temperatures and salinities. This follows from plotted temperature (T), salinity (S), and dissolved oxygen (O_2) at 170 m depth of the central EGB station in Fig. 3. Its position is shown in Fig. 1 and Fig. 2. This interim period lasted 16 years. During that time, relatively smoothed curves describe interannual changes not only in temperature and salinity but also in dissolved oxygen, at least at 170 m depth. Comparing these plots, it seems to be that the inflow event of 1976 was one of the 'late autumn - early winter type'. It reveals a clear correspondence between increasing temperatures and salinities without a significant response in dissolved oxygen. The inflow event of the winter 1992/93 confirms the 'late winter - early spring type' with a significant renewal of oxygen conditions. Thereafter, the salinity reached a relative peak value of about 12.3 psu in winter 1997/98. The temperature increased to a relative maximum of about 6.4° C with a delay of about 18 months without any subsequent improvements in oxygen conditions. These peak values give the potential density of 1009.6 kg/m³ at the pressure level of 170 dbar. In the deep EGB, neighbouring isopycnal

surfaces should be displaced upward due to the deep inflow of warm but highly saline deep water as it is discussed in the following.

The temporal behaviour of the last remarkable inflow could be documented by several data sets. Continuous measurements of salinity and current result from the Darss Sill station while the wind data were recorded at the meteorological station Arkona. Sea level records of the stations Viken (V), Klagshamn (K), and Landsort (L) follow the Swedish coast line. All station positions are shown in Fig.1. Resulting sea level differences ($\Delta\eta$) between the southern Kattegat (station 'Viken') and the south-west Baltic Sea (station 'Klagshamn') control the barotropic part of in- and out flows from the North Sea into the Baltic Sea and vice versa. So, the time history $\Delta\eta(t)$ of resulting sea level differences between Viken $[\eta_V(t)]$ and Klagshamn $[\eta_K(t)]$ determines the net volume tran-

variations at a representative Proper reaction proportional straits.

of sea level of $\eta_L(t)$ are of the Baltic expected to be ss the Danish

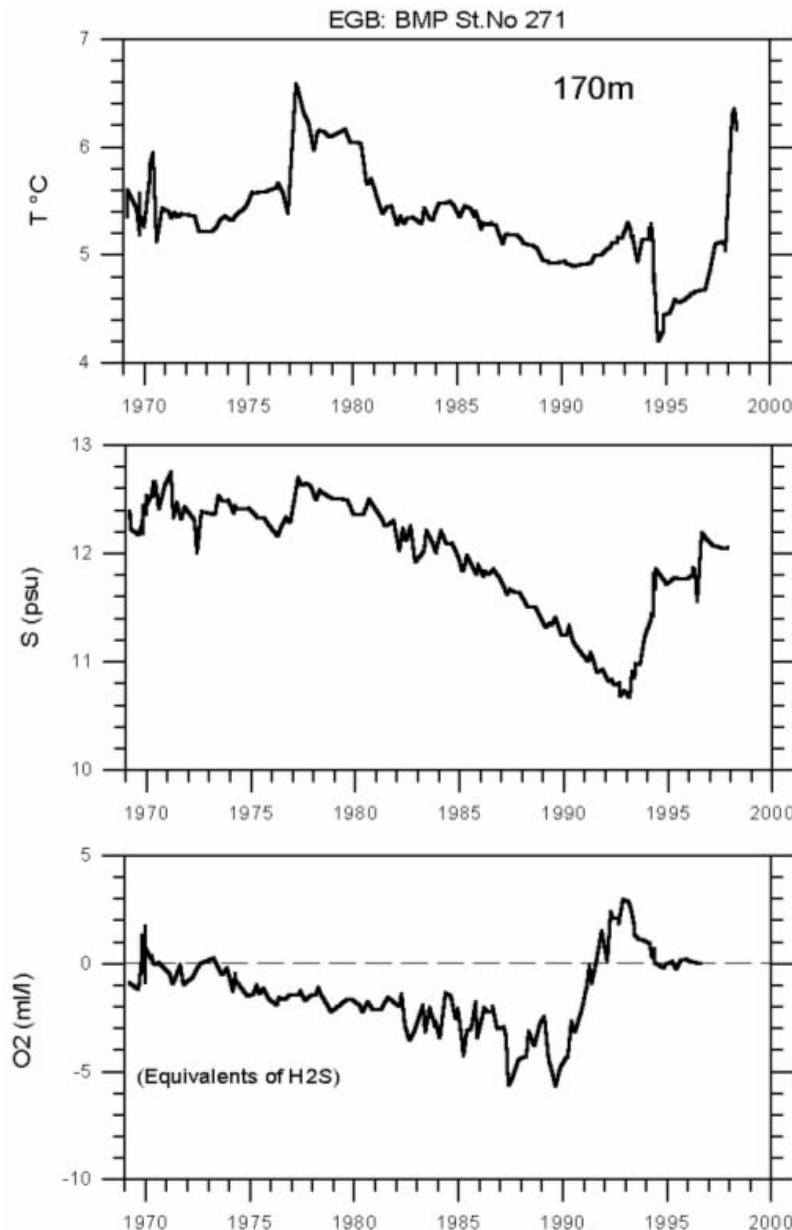


Fig.3 Time series of temperature (T), salinity (S), and dissolved oxygen (O_2) (negative values are equivalents to hydrogen sulfide) at 170 m depth in the central Eastern Gotland Basin; linearly interpolated data result from measurements around UNESCO standard depths at the station 271 (J1) of the Baltic Monitoring Programme (BMP) coinciding with the former Baltic Year station BY15A.

Taking into account the mean freshwater input (F) per unit time, the general balance reads

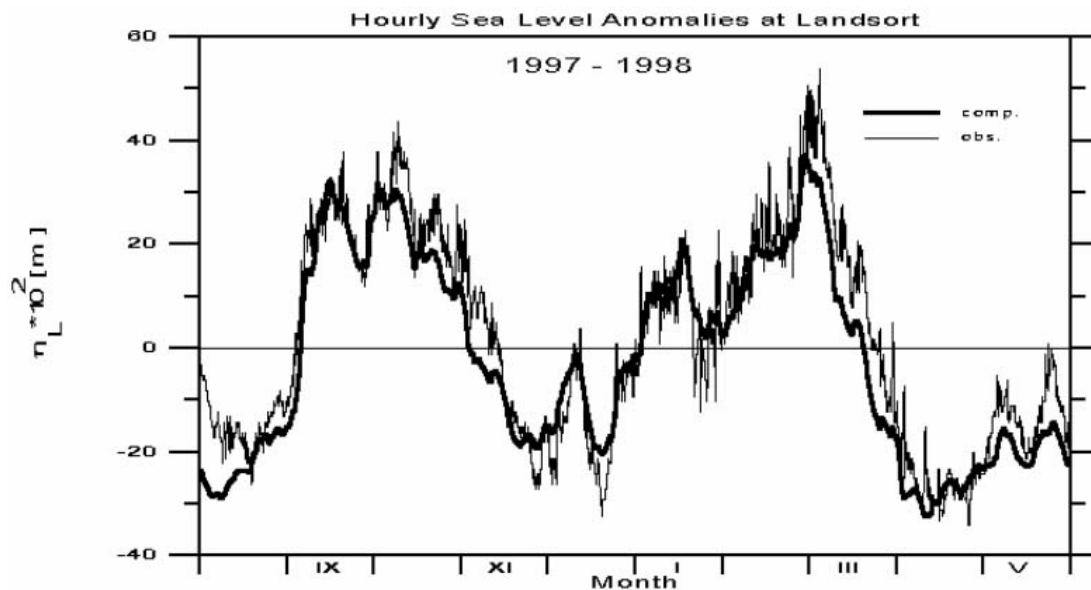
$$d\eta_L/dt = F + G * \Delta\eta(t).$$

The transfer coefficient ($1/G$) describes the characteristic time scale of the net flow through all straits connecting the southern Kattegat with the south-west Baltic Sea. This follows from

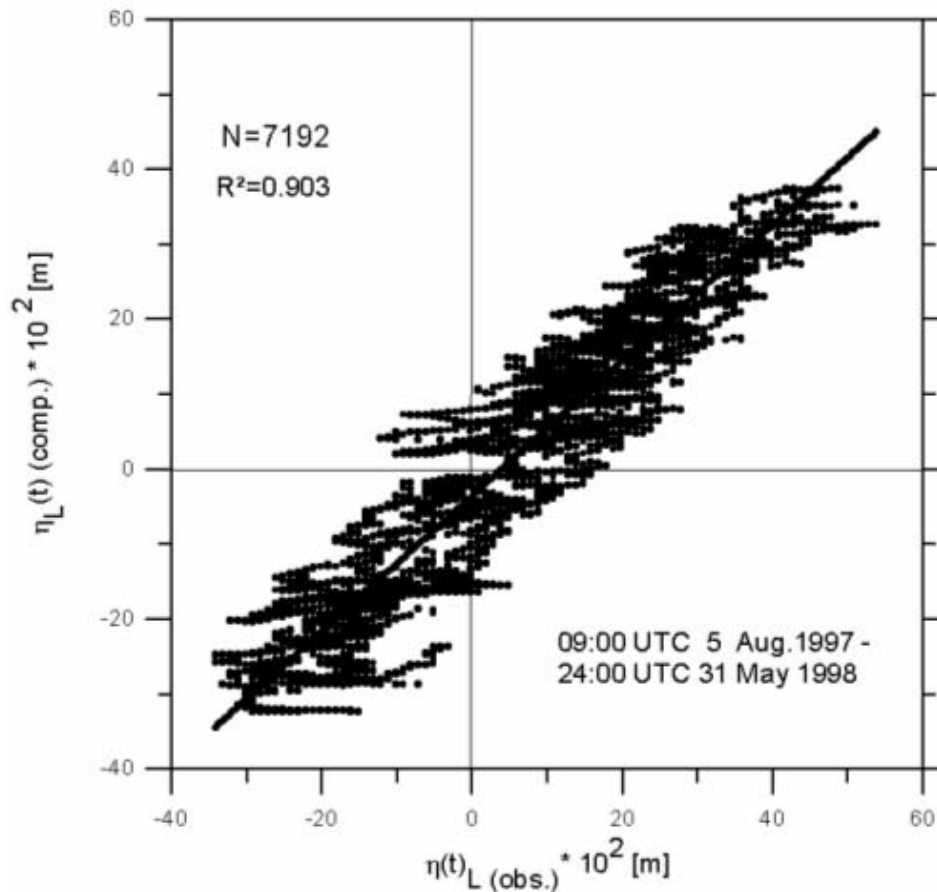
$$\eta_{L,comp.}(t) = \eta_{oL} + F * t + G * \int \Delta\eta(t') dt'.$$

Here, the coefficients are given by $\eta_{oL} = -0.2364$ m, $F = 8.311 * 10^{-3}$ m/d, and $G = 0.1086/d$.

Curves of observed sea level anomalies at the station Landsort $\eta_{L,obs.}(t)$ and computed sea level anomalies $\eta_{L,comp.}(t)$ are drawn in Fig.4a. The qualitative and quantitative coincidence of both curves supports the relevance of the estimated coefficients (F) and (G). The associated scatter diagram reveals a squared correlation coefficient of $R^2 = 0.9$ (Fig.4b). That means 90% of all temporal changes in sea level anomalies at station Landsort were explained without any significant delay (few hours) by the net input of fresh water and changes in the barotropic flow through the transition zone formed by the Sound and the Belts. The rms error of $\eta_{L,obs.}(t)$ was about ± 0.2 m while the mean standard deviation of the difference between $[\eta_{L,obs.}(t) - \eta_{L,comp.}(t)]$ was smaller by the factor of about three. The ratio between the total fresh water input (F) and the transfer coefficient (G) yields $F/G = 0.076$ m. This value coincides with that of the mean sea level difference $\langle \Delta\eta \rangle = \langle (\eta_K - \eta_V) \rangle = 0.076$ m. Obviously, series of $\eta_{L,comp.}(t)$ sufficiently describe those of $\eta_{L,obs.}(t)$. Furthermore, it reveals that the level of the south-west Baltic Sea was somewhat higher than that of the Kattegat. Such an inclination in sea level results from the wind forcing, which acts on the whole basin for relatively short times (days, several weeks), as well as from the net outflow lasting for longer time scales (several months).



4a



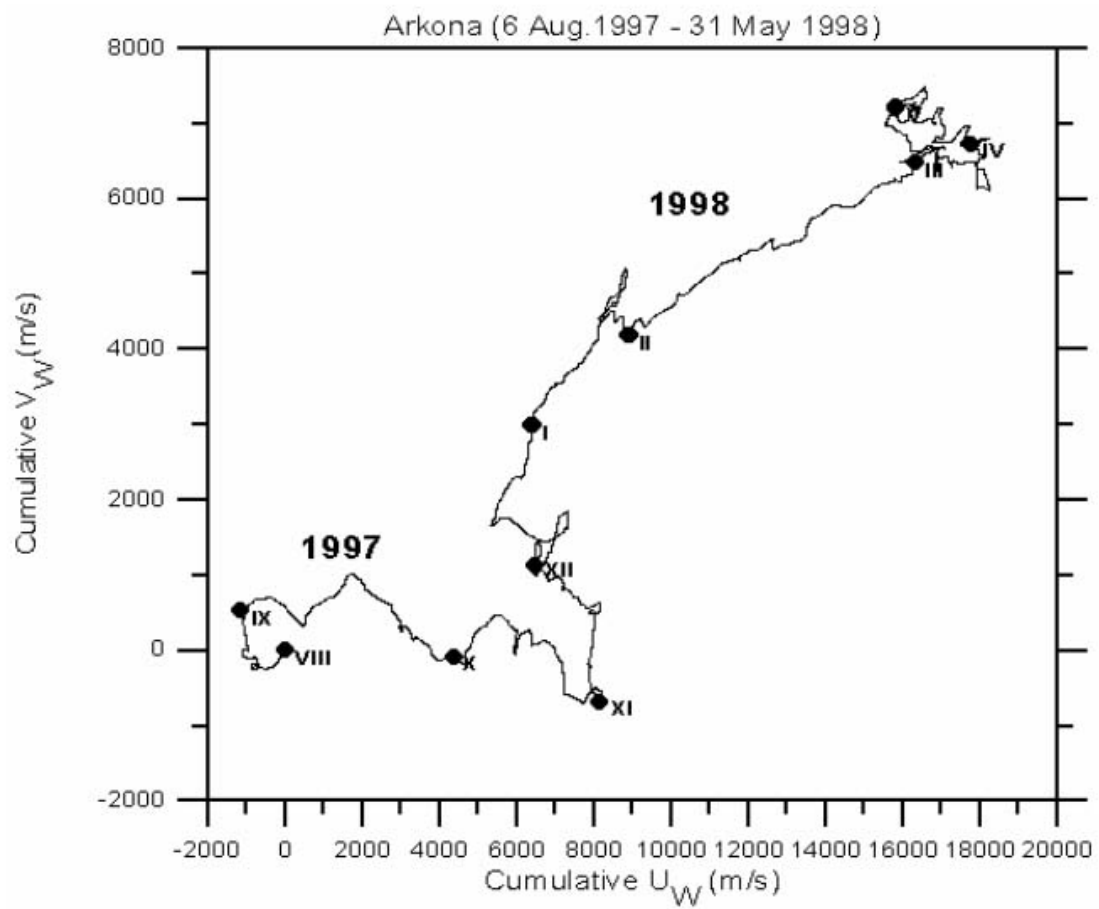
4b

Fig.4 Hourly records of the observed $\eta_{L, obs.}(t)$ and computed $\eta_{L, comp.}(t)$ sea levels with respect to the Swedish Height System 1970 (RH70) at station Landsort from August 5 09:00 UTC, 1997, until May 31 24:00 UTC, 1998

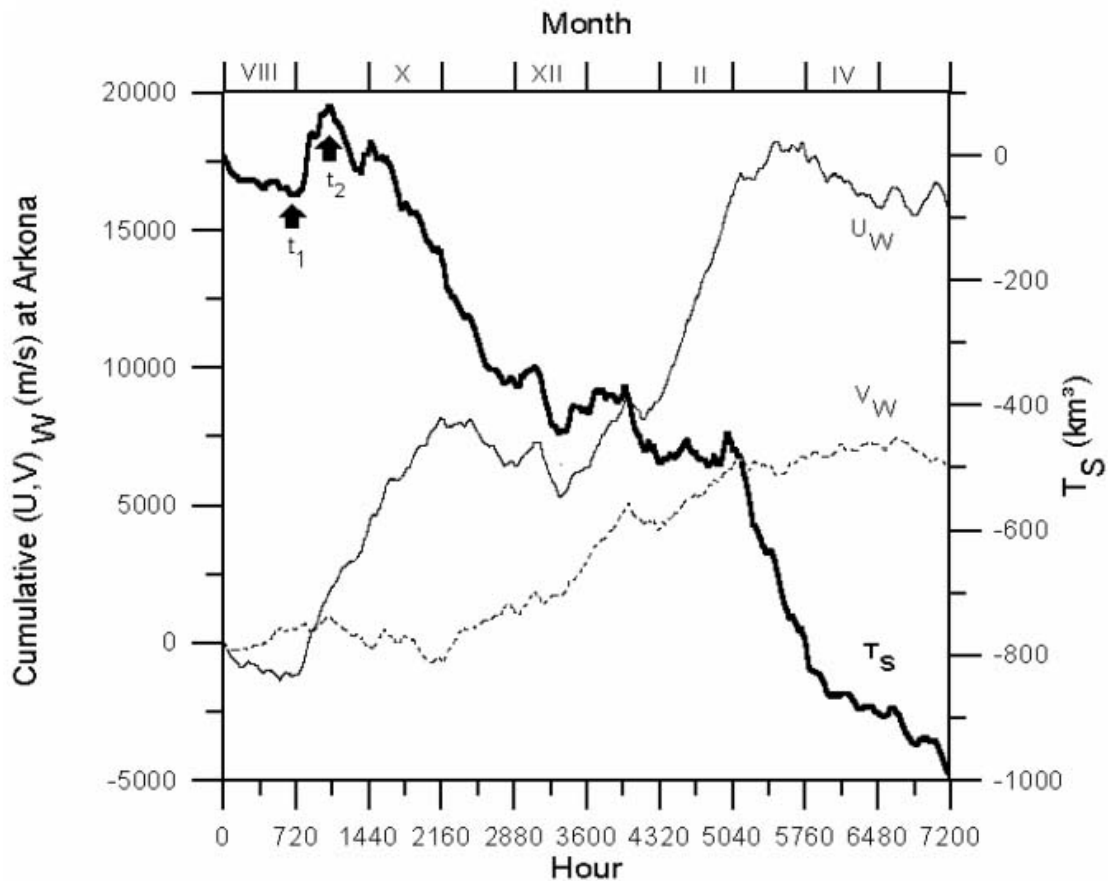
- a) time plots of $\eta_{L, obs.}(t)$ (thin line) and $\eta_{L, comp.}(t)$ (bold line)
- b) scatter diagram between $\eta_{L, obs.}(t)$ and $\eta_{L, comp.}(t)$ for $N= 7192$ values and the squared correlation coefficient $R^2= 0.903$; the straight line indicates the linear regression described in the text.

Following MOHRHOLZ (1998), we assume that wind records of the station Arkona are representative for large Baltic regions because horizontal scales of atmospheric forcing fields exceed the basin scale of the whole Baltic Sea. The time history of the wind field is given by a progressive vector diagram of hourly Arkona winds in Fig.5a. Tick marks indicate each beginning month by Roman numbers. This plot reveals the direction into the wind was blowing. Increasing distances between adjacent tick marks indicate increasing wind velocities. Southerly winds predominated the August 1997. The wind turned to western directions in September. It maintained this direction until the end of October to turn again into the southern sector with the beginning November. Northward blowing winds lasted until March 1998 to indicate increasing wind velocities during the whole February 1998. Thereafter, the wind relaxed to fluctuate in both direction and velocity. Consequently, relatively long lasting periods with pronounced wind directions essentially influenced lateral inclinations in sea level anomalies across the whole Baltic Sea. Thus, we like to accept that the time series of $\eta_{L, comp.}(t)$ sufficiently represent changes in the water volume of the entire Baltic Sea via $A * \eta_{L, comp.}(t)$ with $A = 382\,486 \text{ km}^2$ being the surface area of the Baltic Sea. This value of A completely excludes the Kattegat. The calculation

procedure uses new information about Baltic shore lines and is described more in detail in the Appendix II, which also includes Fig.A1 showing the defined boundaries.



5a



5b

Fig.5 Wind recorded at the northern top of the Ruegen island (Fig.1) in comparison to the net volume flux through Danish straits:

- a) Progressive vector diagram composed by cumulative zonal winds (U_w) and corresponding meridional winds (V_w) pointing to the direction into the wind was blowing [positive to the east (E) and to the north (N)]; Roman numbers indicate the beginning month starting in August 1997 and ending in May 1998.
- b) Hourly time series of U_w (thin line), V_w (dotted line), and the net volume flux through Danish straits (T_s) (bold line) obtained from fitted sea level variations at Landsort (details in the text); the arrows t_1 and t_2 indicate starting and ending time of the inflow, which is marked by positive values of T_s ; note the opposite correspondence between $U_w(t)$ and $T_s(t)$.

Accepting mentioned assumptions, the total water volume of the Baltic Sea results from the balance between net transports through the Danish straits $T_s(t)$ and the total input of fresh water ($A * F * \Delta t$) during the time interval Δt . Consequently, the resulting volume flux reads

$$\Delta T_s(t) = A * [\Delta \eta_{L,comp}(t) - F * \Delta t].$$

The obtained curve $T_s(t)$ is compared with cumulative winds of the Arkona station in Fig.5b and separately drawn in the upper panel of Fig.6. Its negative trend confirms a permanent surplus of brackish water for that time period and $T_s(t)$ oppositely corresponds to $U_w(t)$. This suggests that, via changed sea levels between the south Kattegat and the south-west Baltic Sea, the net flow through Danish straits was mainly controlled by the time history of westerly winds.

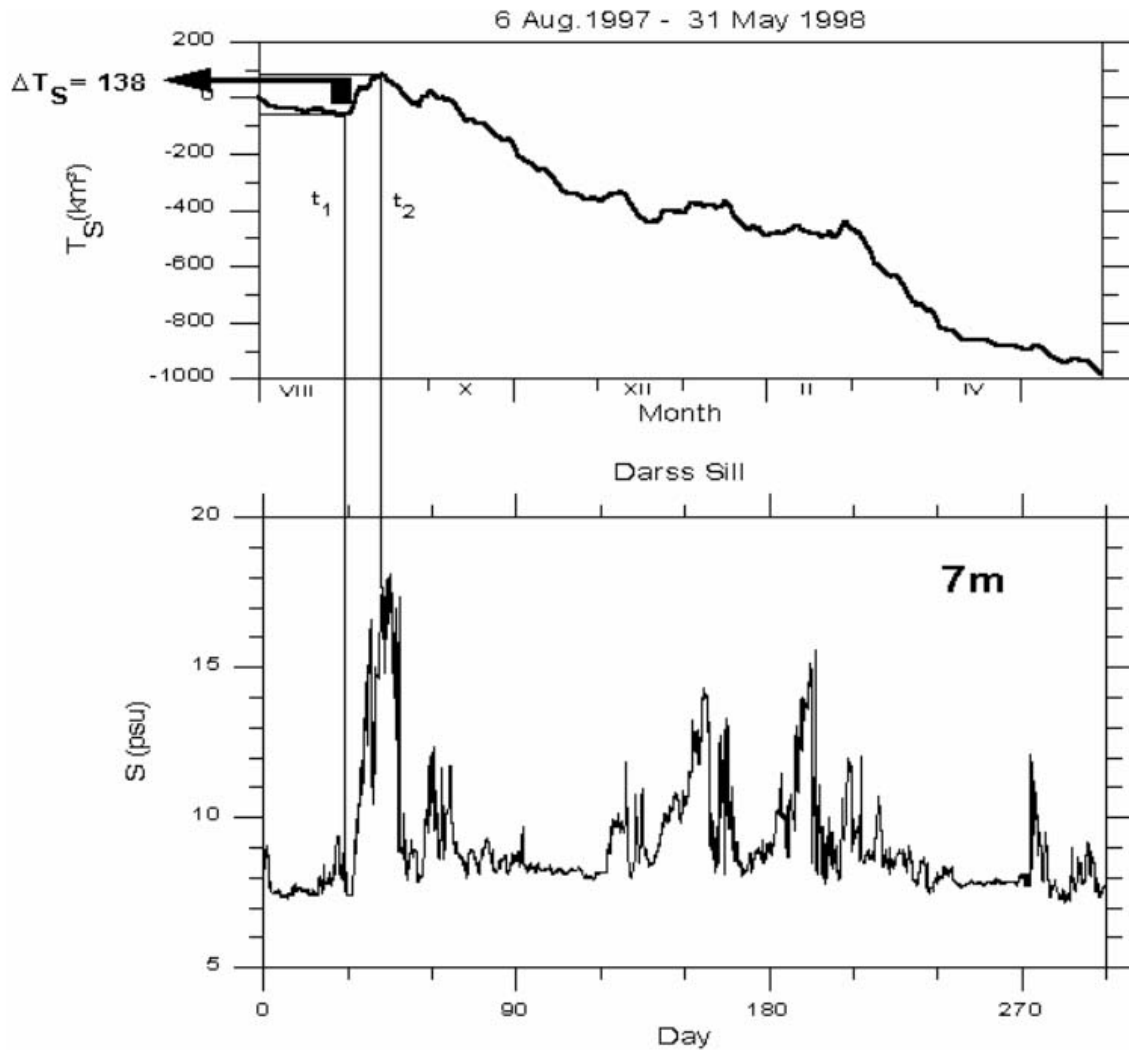


Fig.6 Estimated net volume flux through Danish straits (Belts and Sound) as in Fig.5b with the inflow of about $\Delta T_S = 138 \text{ km}^3$ water in the beginning September 1997 (upper panel) in comparison with the salinity (S) observed at 7 m depth at the Darss Sill (lower panel); note relatively small gradients $\Delta T_S / \Delta t > 0$ correspond to relative peak values in $S(t)$; thin vertical lines of both t_1 and t_2 reveal the delay of several days between $T_{S,\min}(t_1)$ and $S_{\min}(t_1)$ as well as between $T_{S,\max}(t_2)$ and $S_{\max}(t_2)$.

The inflow event started with a relative minimum $T_{S,\min}(t_1)$ on September 04 (21:00 UTC) and ended with a relative maximum $T_{S,\max}(t_2)$ on September 18 (14:00 UTC), 1997. Therefore, it lasted $\Delta t = 329 \text{ h} = 13.7 \text{ d}$ and exceeded the characteristic time of the net flow through the Danish straits $(1/G) = 9.2 \text{ d}$ by the factor of about 1.5. This was a sufficient precondition for an effective inflow, which is able to influence the whole south-west Baltic Sea. Its saline water reached the Darss Sill with a pronounced maximum in salinity $S_{\max} = 18.13 \text{ psu}$ at 7 m depth on September 19, 22:00 UTC. Both plots indicate a delay of about 15 days between $T_{S,\max}(t_1)$ through the Danish straits and S_{\max} observed at the Darss Sill. The difference $\Delta T_S = T_S(t_2) - T_S(t_1)$ estimates the mean inflow volume to be $\Delta T_S = 138 \text{ km}^3$ as it is shown in the upper panel of Fig.6. The associated mean volume transport $\Delta T_S / \Delta t$ was about $10 \text{ km}^3/\text{d}$. During the inflow time of $\Delta t = 13.7 \text{ d}$, the total fresh water input was $(A * F * \Delta t) \approx 43.6 \text{ km}^3$ with a mean volume

transport of about $3.2 \text{ km}^3/\text{d}$. Thus, the volume transport of the net inflow was more than three times larger than that of the estimated total input of fresh water. Such volume fluxes are comparable with those reported by JAKOBSEN (1995) and MATTHÄUS and LASS (1995) from the winter 1992/93. That inflow transported between 135 km^3 and 154 km^3 saline deep water towards the Baltic Sea. It lasted about 21 days. Associated transports reached values between $6.4 \text{ km}^3/\text{d}$ and $7.3 \text{ km}^3/\text{d}$. According to JAKOBSEN (1995), only 1/7 of the water masses passed the Sound. Relatively cold ($3.5 \text{ }^\circ\text{C}$), highly saline ($S > 17 \text{ psu}$), and well oxygenated water ($\text{O}_2 > 8 \text{ ml/l}$) overflowed the Darss Sill in the western Baltic. The content of dissolved oxygen reached peak concentrations of about 3.5 ml/l in layers beneath the perennial halocline of the EGB. No comparable values of dissolved oxygen were observed during the winter 1997/98 because that inflow was one of the 'late autumn - early winter type'.

At the Darss Sill station, the temperature of the 7 m horizon decreased from 20.8°C (September 5) to 15.3°C (September 19) in response to this inflow event. Simultaneously, the salinity increased from 7.4 psu to about 17 psu . This follows from SeaCat records providing the 'progressive T-S plot' drawn in Fig. 7. Final values of 15.3°C , 17 psu , and 7 dbar yield the density of 1012.1 kg/m^3 . That means relatively dense water covered the whole water column over the Darss Sill to spread towards the next deep basin, the Arkona Basin.

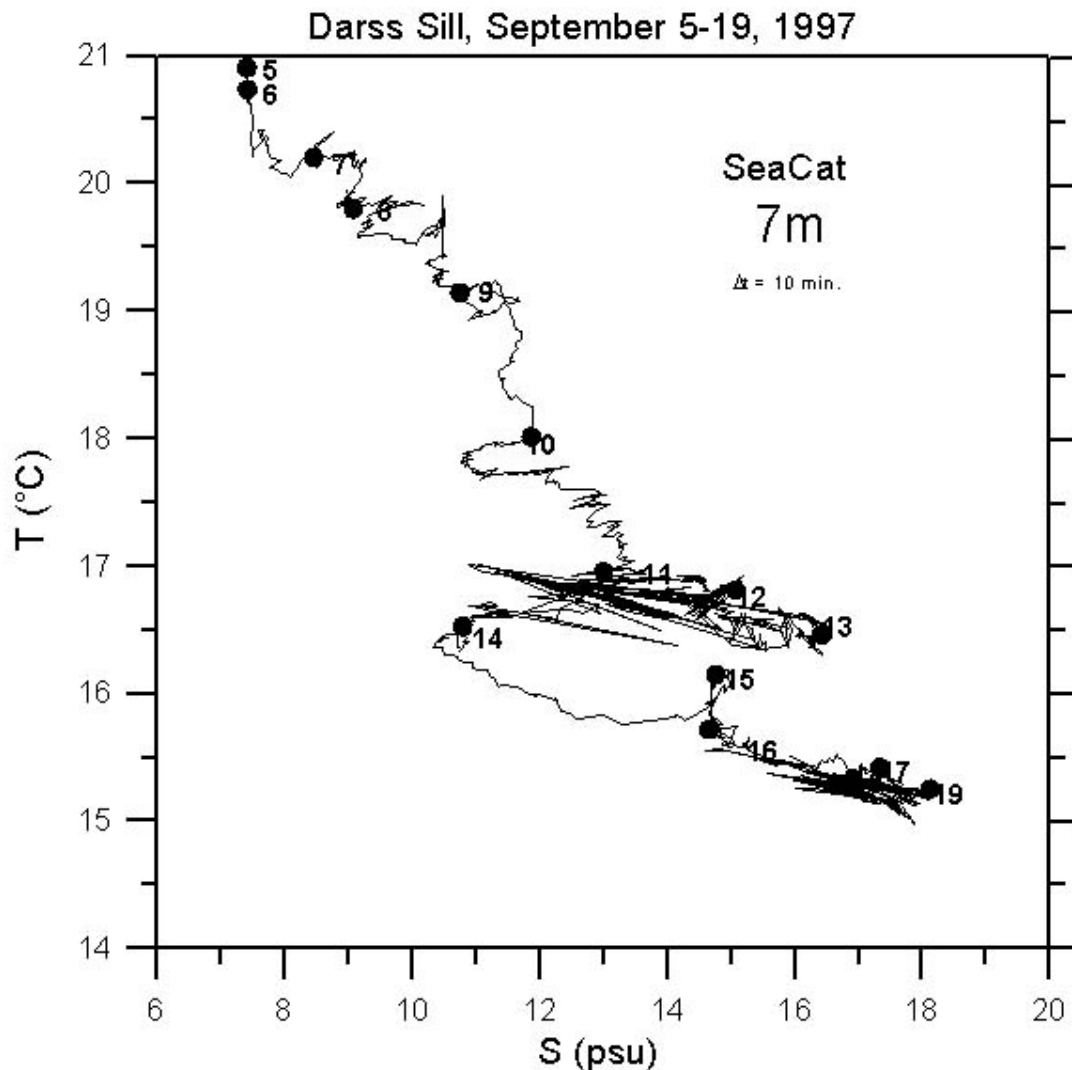


Fig.7 Temperature (T)- Salinity (S) relationship at 7 m depth measured by a SeaCat recorder with the sampling frequency of $\Delta t = 10$ minutes at the Darss Sill during 14 days in September 1997; dots indicate the beginning day.

This eastward spreading was released/ maintained by westerly winds. This follows from hourly arrows of Arkona winds in the upper panel of Fig.8. Such winds generated eastward motions within the whole water column above the Darss Sill. Related current arrows are drawn from measurements at 7, 12, 17, and 19 m depth in the lower panels. For example, hourly mean values of eastward currents reached peak values of about 50 cm/s at 12 m depth during the 14 d lasting passage of the inflow event. That means an unknown amount of saline water overflowed the Darss Sill during the mentioned two weeks in September 1997 to propagate farther eastward. Here, we may expect that this inflow event continued to reach the EGB.

Above topographic flanks of the EGB, temperature was recorded beneath the perennial pycnocline at 140 m, 155 m, and 170 m depth at positions denoted by NE and SW in Fig.2. Plots of daily averages and associated variances are drawn in Fig.9 and Fig.10. Five daily running means are used to suppress fluctuations of the synoptic time scale in the following. The inflow signal reached the level of 170 m at the NE position on November 28, but at the SW position on December 28, 1997.

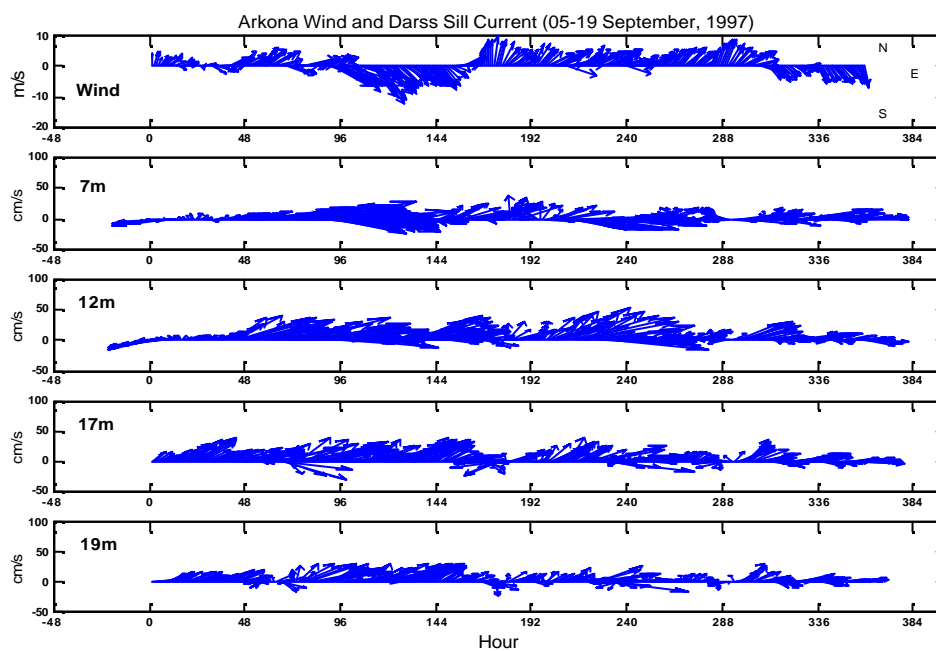


Fig.8 Hourly arrows of Arkona winds in comparison with those of currents above the Darss Sill at 7, 12, 17, and 19 m water depth during the inflow period in September 1997; cf. Fig.1 for station locations.

That means the inflow signal needed about 70 days to propagate over the distance of about 650 km from the Darss Sill to the NE position in the EGB. Thus, it results a mean eastward velocity of about 10 cm/s.

The temperature records show for all three horizons similar curves for averages and variances at both positions although the variance levels are significantly lower at the SW position. These plots demonstrate that the thermal regime reacted nearly simultaneously within the layer between 140 m and 170 m at both moorings during the whole recording time. Related statistics, which are based on hourly and half hourly values, are compared with those of daily averages in the Table 3.1.. Daily means underestimate total variances of about 7-8 % at both positions. Independently of the horizon, daily averages smooth the range between measured peak values (maximum-minimum) by about 14% at the position NE but by about 24% at the SW-position. Nevertheless, we like to confine further considerations on time series based on daily averages and daily variances. Curves of daily averaged temperatures visually show at least three characteristic periods at both moored strings in Fig.9a and Fig.10a. As it will be shown later, the first one describes pre-inflow conditions. It is marked by nearly constant temperatures around 5°C. During December 1997 until March 1998, the temperature linearly increased to about 6°C. This is the second period. Its trend lasted about 130 days at the NE-position but 120 days at the SW-position. The associated inflow established vertical temperature gradients and daily variances reached their maximum. Triggered mixing processes probably stabilised the temperature regime of subsequent time periods. After April (NE position) and May (SW position), nearly constant temperatures were recorded with values fluctuating around 6°C.

Daily variances (σ^2_{τ}) show a decreasing trend at both positions during the third period. All three time-periods have been identified by the criterion $\sigma^2_{\tau} < 0,05 K^2$, which sufficiently distinguishes between pre- and post-inflow situations and the inflow period. Resulting time segments are gathered in Table 3.1. while basic statistics of all available temperature series are compiled in Table 3.2..

Series	NE			Daily		
Depth (m)	140	155	170	140	155	170
Time	30.8.97- 21.7.98	30.8.97- 13.5.98	30.8.97- 21.7.98	30.8.97- 21.7.98	30.8.97- 13.5.98	30.8.97- 21.7.98
N	15648	10896	7824	326	227	326
Mean /°C	5.56	5.39	5.61	5.56	5.39	5.61
$\sigma^2 (K)^2$	0.298	0.270	0.227	0.276	0.240	0.207
Min. (°C)	4.75	4.80	4.89	4.79	4.87	4.92
Max. (°C)	7.28	7.43	7.51	6.89	7.17	6.90
Range (K)	2.53	2.63	2.62	2.10	2.30	1.98

Series	SW			Daily		
Depth (m)	140	155	170	140	155	170
Time	30.8.97- 8.11.98	30.8.97- 8.11.98	30.8.97- 14.9.98	30.8.97- 8.11.98	30.8.97- 8.11.98	30.8.97- 14.9.98
N	20928	20928	9144	436	436	381
Mean /°C	5.45	5.65	5.68	5.57	5.65	5.68
$\sigma^2 (K)^2$	0.219	0.212	0.220	0.193	0.205	0.214
Min. (°C)	4.80	4.83	4.92	4.87	4.95	4.98
Max. (°C)	6.78	6.90	6.98	6.39	6.54	6.59
Range (K)	1.98	2.07	2.06	1.52	1.59	1.61

Table 3.1.

Statistics of temperature series resulting from half hourly (140m, 155m) and hourly samples (170m), which were recorded from 30 August 1997 until 21 July 1998 in layers beneath the permanent halocline at the position NE but until 14 September 1998 (170m) and 8 November 1998 (140m, 155m) at the position SW; the number of records is N, daily averages are based on values between 00:00 and 23:30 UTC and point to 12:00 UTC, variances are given by σ^2 while minimum (Min.) and maximum (Max.) determine the total range of measured changes; peak values of each row are given by bold numbers.

At both positions, the pre-inflow period (A) and both post-inflow periods (C, D) indicate relatively small daily variances fluctuating around zero in Fig.9b and Fig.10b. Associated statistics are given for each identified time segment in Table A.1 of the Appendix I. The period (A) of pre-inflow conditions lasted 90 days at the position NE but 120 days at the SW position. Mean temperatures were somewhat higher in the SW than in the NE and slightly fluctuated around a constant value at both positions. Nevertheless, the total mean of the vertical gradient was about $4 \cdot 10^{-3} K/m$ within the layer between 140 m and 170m depth at both positions.

These conditions dramatically changed from segment (A) to segment (B). The period (B) was characterised by the inflow of warm but dense deep water. It reduced the vertical temperature gradient by a factor of about two within the layer between 170 m and 140 m. This reduction indicates a vertical homogenisation of the deep temperature field. The period (B) also shows linearly increasing temperatures with enhanced variance levels. Both parameters drastically

fluctuate in time at both moorings. Six significant peak values were superimposed on this trend. All relative peak values were more pronounced at the NE position than at the SW position. Their averaged period of about 22 days revealed the mean amplitude of 0.3 K at the NE position.

Position/ Days	NE	N	SW	N
A: Pre-inflow (V, T)	30.08.1997- 27.11.1997	90	30.08.1997- 27.12.1997	120
B: Inflow (V, T)	28.11.1997- 06.05.1998	130	28.12.1997- 26.05.1998	120
C: Post-inflow (V, T)	07.05.1998- 21.07.1998	106	27.05.1998- 04.08.1998	100
D: Post-inflow (V) (T)	No Data	No Data	05.08.1998- 14.09.1998 08.11.1998	41 96
Total Current (V) Temp. (T)	30.08.1997- 21.07.1998	326	30.08.1997- 14.09.1998 08.11.1998	381 436

Table 3.2.

Identified time segments in temperature records (T) and those of current measurements (V) of N days at the positions (NE) and (SW).

This value was reduced by the factor of about two at the SW position. High frequency temperature fluctuations with periods shorter than the daily cycle, which are given by daily variances, also exhibit higher energetic levels at the NE position than at the SW position. Obviously, there was a significant loss in the level of high frequent temperature variations on the path way from mooring the NE to the mooring SW. The level of daily variances was at least one magnitude larger during the inflow period (B) than during the pre-inflow period (A) and during both post-inflow periods (C, D). That suggests that inflow events drastically control the energetic level of high frequency fluctuations, which are mirrored by changes in the deep temperature field. The last row of Table A.1. shows that the total fluctuation between minimum and maximum was generally larger in NE than in SW. Here, we only conclude that the energetic level of all fluctuations was significantly higher at the mouth of the inflow and damped out significantly on the path way towards the SW mooring.

At the NE position, the warm water reached the 170 m level about ten days earlier than the 140 m horizon, Fig. 9a. This difference yields a mean upward directed velocity of about $3.5 \cdot 10^{-5}$ m/s for the beginning inflow period. The delay was only seven days at the SW-position as shown in Fig. 10a. Here, the averaged upward velocity was about $5 \cdot 10^{-5}$ m/s. Any upward lifting of water, which was trapped within such deep layers, drastically relaxed during post-inflow periods. The post-inflow period (C) lasted 106 days at the NE-position but 100 days at the SW-position. The level of its daily variances is also one magnitude lower than that of the inflow period (B). This suggests that the thermal regime of the post-inflow period (C) was somewhat better homogenised than that of the inflow period (B) but, following Fig.9b and Fig.10b, not in the same degree than that of the pre-inflow period (A). Due to the greater recording length at the SW-position, we additionally identified the time-segment (D) with 96 days. In layers between 170 m and 140 m depth, its daily temperatures fluctuated between 10 and 20 days around an aspired equilibrium temperature of about 6.2°C .

The plot of Fig. 10a also shows a local cooling of about 0.7 K at 155m depth in the early

September, 1998. After a careful inspection of the original data, we like to exclude any instrumental errors. That means there was the passage of a shallow cold water plume. It influenced the thermal regime for the duration of about two weeks in between 140 m and 170 m depth.

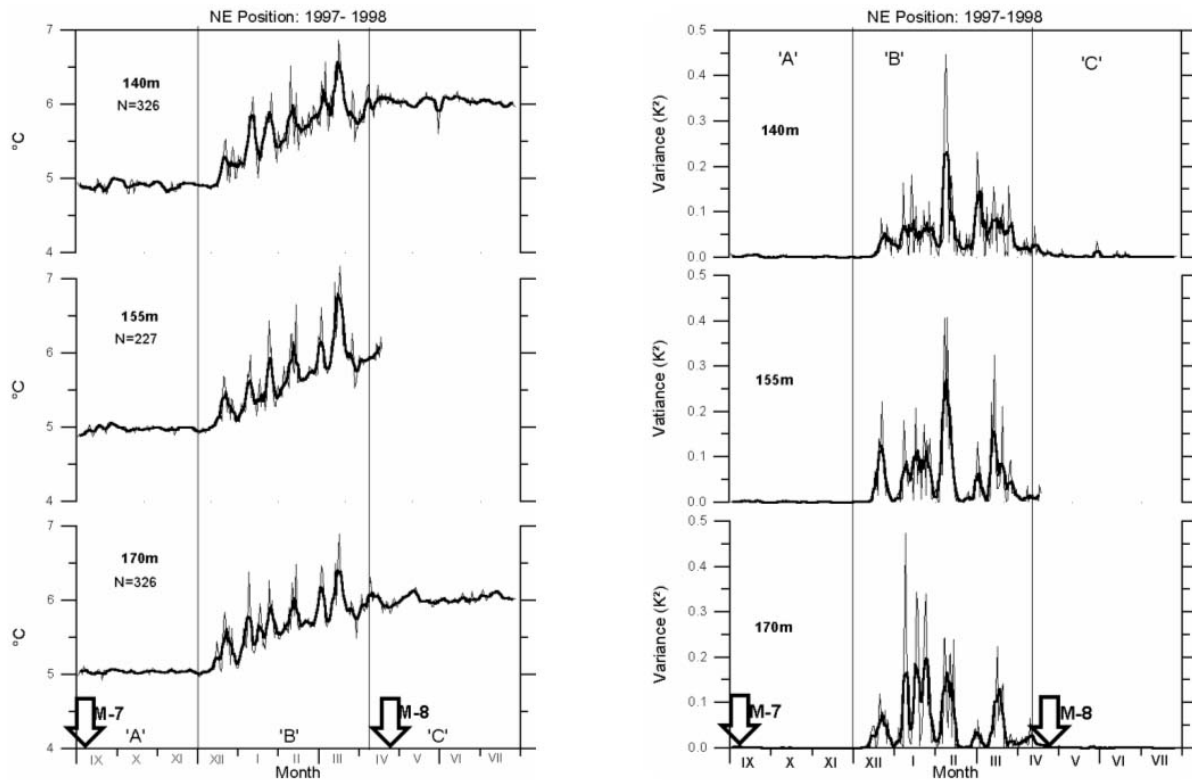


Fig.9 Temperature records ($^{\circ}\text{C}$) at 140 m, 155 m (Seamon-Mini, sampling interval = 0.5 h) and 170 m depth (Aanderra, sampling interval = 1 h) at the NE position ($57^{\circ}25.38'\text{N}$, $0^{\circ}20.83'\text{E}$) versus time; the width of downward directed arrows indicates time windows of both the MESODYN-7 (M-7) and the MESODYN-8 (M-8) field campaigns;

- daily averages (thin lines) and their five daily running means (bold lines); the total length is given by N days; identified time segments are separated by thin vertical lines indicating the pre-inflow situation 'A', the inflow situation 'B', and the post-inflow period 'C',
- as in (a) but for daily variances.

Simultaneously, daily variances increased drastically in Fig.10b (cf. enhanced mean kinetic energies in Fig.12b). Such observations suggest that layers between 140 m and 155 m depth can be influenced sporadically by features, which mix cold water of intermediate and/ or upper layers with relatively warm deep water.

North-westward flowing currents dominated the motion field during the entire observational period at 170 m depth above the eastern topographic flank. This follows from the progressive vector diagram (PVD) plotted for the NE position in Fig. 11. The mean current velocity was 3.5 cm/s towards the north-west sector during the whole recording time of 326 d. The corresponding

plot for the SW position covers 381 days. It shows a mean velocity of 3.2 cm/s into the south-east sector. Thus, both plots suggest the existence of a cyclonic circulation. It probably followed lines of constant water depth in deep parts of the EGB. Increasing distances between 30-day tick-marks indicate that this circulation significantly accelerated during the inflow-period (B) at both mooring positions. By contrast to the straight PVD to north-west at the NE position, motions rhythmically fluctuated on smaller zonal scales at the SW position. Associated statistics of current components are tabulated for actual measurements and daily means in Table. 3.3..

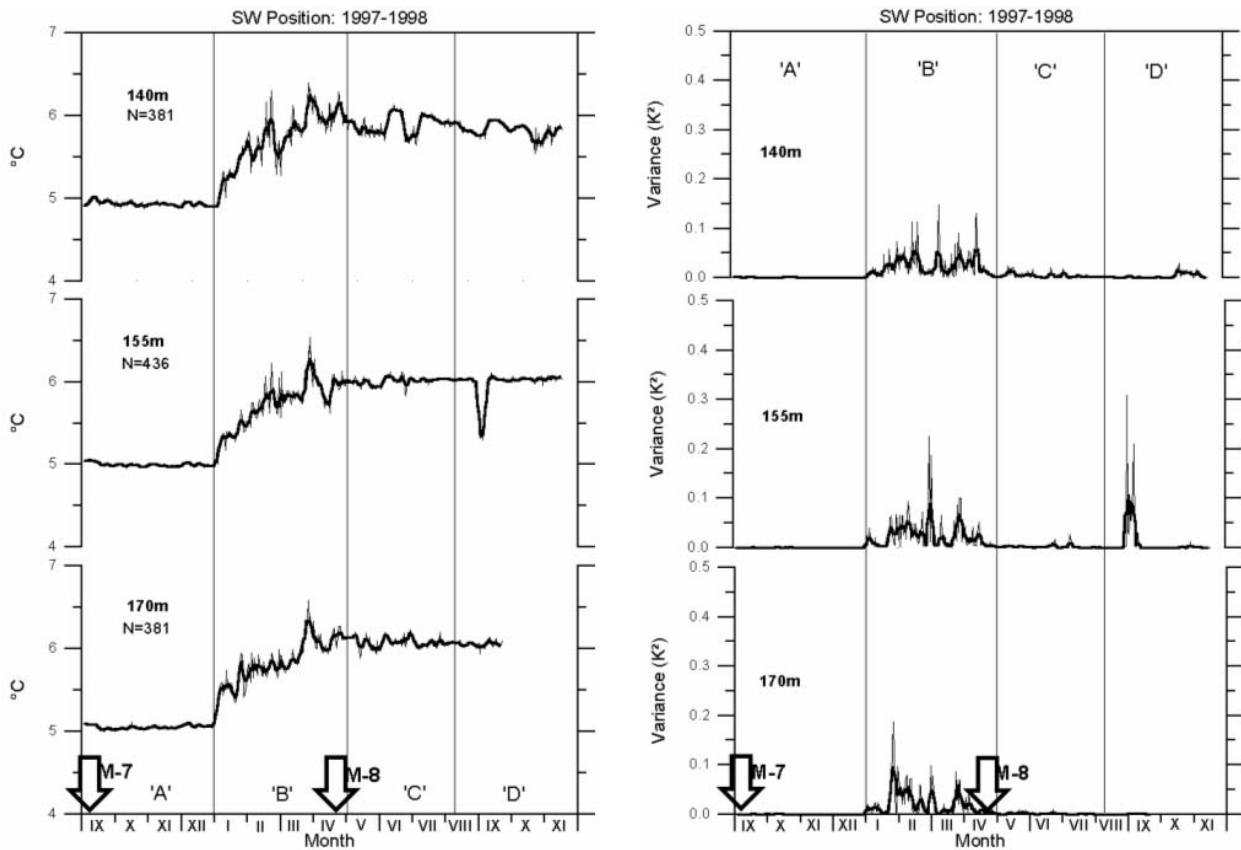


Fig.10 As in Fig.9 (a, b) but for the SW position ($57^{\circ}04.53'N$, $19^{\circ}45.12'E$).

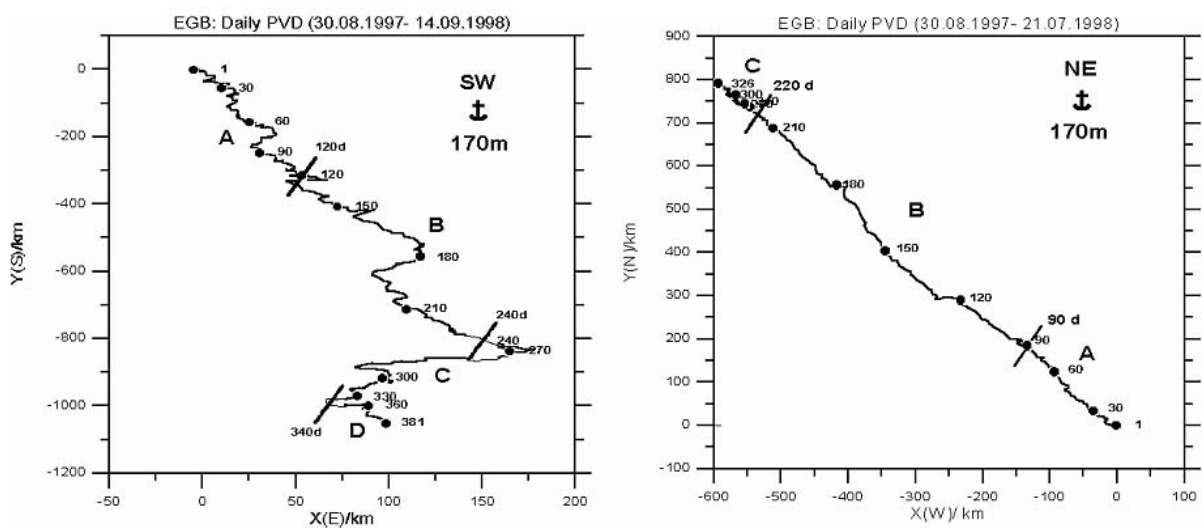


Fig.11 Progressive vector diagram (PVD) of daily averages of zonal and meridional current components with tick marks every 30 days (dots); the identified periods 'A', 'B', 'C', and 'D' are separated by bold lines; abscissa and ordinate indicate apparent path-ways; note different scales along the abscissa :

- N= 381 days at the SW position (57°04.53'N, 19°45.12'E),
- N= 326 days at the NE position (57°25.38'N, 20°20.83'E).

It became evident that daily averages underestimated variances of both components by about 35% at the NE-position but by about 42% at the SW-position. More in general, the level of total variances in the meridional component (v), which roughly indicated fluctuations parallel to bathymetric contours, was significantly higher than that of the zonal component (u) at both positions. This observation is also confirmed by values of the total fluctuation range between maximum and minimum.

Position	NE				SW			
Series	u-tot.	u-d.	v-tot.	v-d.	u-tot.	u-d.	v-tot.	v-d.
Time	30.8.97- 21.7.98	30.8.97- 21.7.98	30.8.97- 21.7.98	30.8.97- 21.7.98	30.8.97- 14.9.98	30.8.97- 14.9.98	30.8.97- 14.9.98	30.8.97- 14.9.98
N	7824	326	7824	326	9144	381	9144	381
Mean*10 ² m/s	-2.1	-2.1	2.8	2.8	0.3	0.3	-3.2	-3.2
$\sigma^2 \cdot 10^4$ (m/s) ²	15.38	9.62	20.77	13.85	18.80	10.96	25.41	14.82
Min.*10 ² m/s	-21.0	-13.9	-11.0	-7.5	-18.0	-12.9	-29.0	-24.0
Max.*10 ² m/s	11.8	9.9	27.2	19.1	23.4	14.7	13.6	5.5
Range*10 ² m/s	32.8	23.8	38.2	26.6	41.4	27.6	42.6	29.5

Table 3.3.

Statistics of the zonal component (positive to the east) and the meridional component (positive to the north) of current measurements at 170m depth at the NE position and the SW position provided by hourly samples (u-tot., v-tot.) and daily averages (u-d., v-d.); the number of records is N; daily averages are based on values between 00:00 and 23:00 UTC and point to 12:00 UTC; the variance is σ^2 while minimum (Min.) and maximum (Max.) determine the total range of fluctuations.

As it could be expected, the energetic level of MKE was somewhat higher than that of EKE at both mooring positions. That follows from plots shown in Fig.12 (a, b). Their peak values occurred during the inflow period (B) on the scale of several days. Visually, the MKE curve indicates that current fluctuations of the post-inflow periods (C, D) exhibited lower frequency changes than those, which were recorded under pre-inflow conditions (A) at the SW position. At the NE position, the linear regression between logarithmic values of MKE and EKE suggests that energy fluxes from the field of mean kinetic energy into the field of higher frequency fluctuations dominated the inflow period (B). This strong relationship explains 84% of the associated scatter plot. No comparable regressions could be recorded during period (A) and (C) at the NE position and at the SW position at all. Consequently, we conclude that this inflow event intensified high frequency mixing processes to accelerate homogenisation of the thermal regime within layers between 170m and 140m above the eastern flank of the EGB.

Statistics of the current components (u , v), MKE, and EKE are tabulated for all identified time segments in Table A.2. of the Appendix I. This table also confirms that currents accelerated by the factor of about two at both positions during the inflow period (B) to relax again in both post-inflow periods (C,D). Total variances (σ^2) of the mean kinetic energy (MKE) as well as those of the mean 'eddy kinetic energy' (EKE) reached their maximum. The Table 3.2. clearly indicates that the time-segment (B) started 30 days later at the SW position than at the NE position. Consequently, the temperature jump of about 1 K needed this time to overcome the distance between both moorings. Assuming that the path-way of the inflow event followed bathymetric contours along the north-western flank of the EGB then the distance between both moorings was about 64 km. Delay and distance estimate the averaged propagation speed to be 2.5 cm/s. This value confirms the measured mean velocity of 3 cm/s. Along the closed 220 m depth contour, the total circumference is about 130 km. That means the thermal inflow signal needed about 60 days to travel around the whole deep basin for the first time. The correspondence between changes in the thermal field and those of the motion field is shown for the inflow period (B) at NE position by five daily running means of the meridional current component (v) and the temperature (T) in Fig. 13.

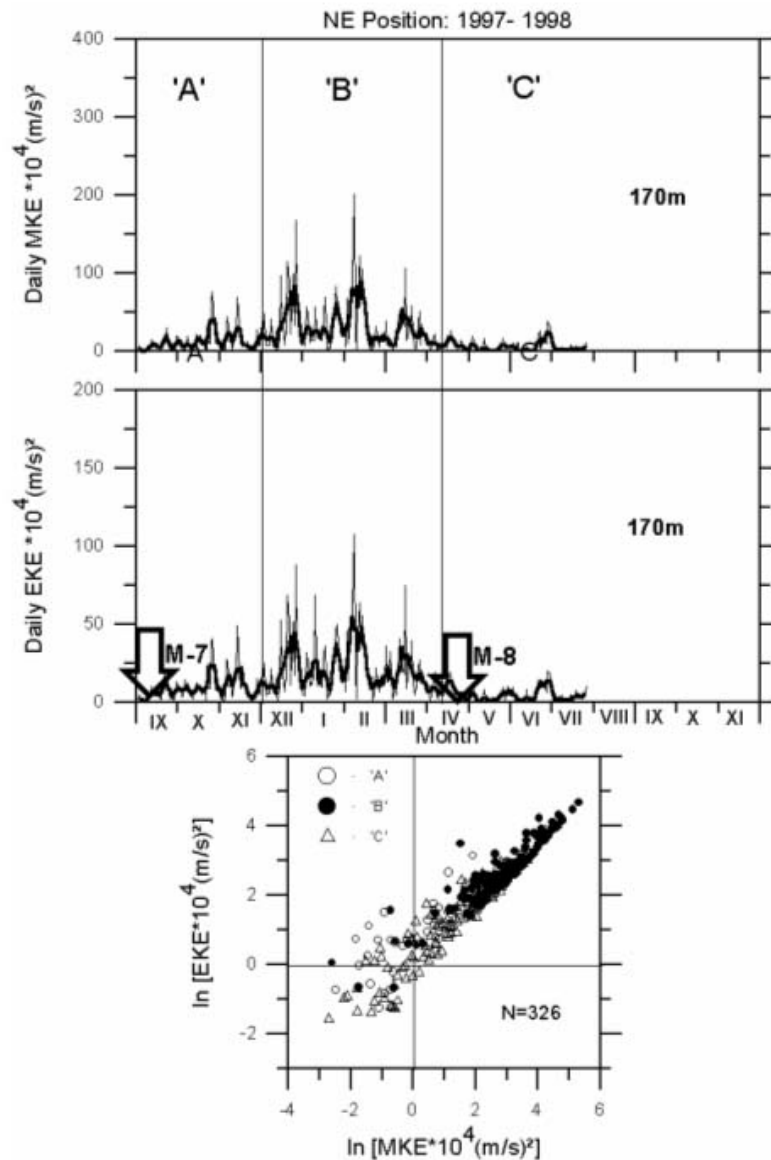


Fig.12 Time series of daily mean kinetic energy [$MKE = (u^2 + v^2)/2$] and daily 'eddy kinetic energy' [$EKE = (\sigma_u^2 + \sigma_v^2)/2$] per unit mass in comparison with the scatter plot between logarithmic values of MKE and EKE; identified periods are distinguished by 'A' (open circles), 'B' (dots), and 'C' (triangles) in the lower panel; arrows indicate the MESODYN campaigns by M-7 (September 1997) and M-8 (April 1998) in the upper panel

a) $N = 326$ days at the NE position ($57^\circ 25.38'N$, $20^\circ 20.83'E$).

Peak values of both parameters coincide visually. The maximum of northward currents fluctuates between 5 cm/s and 10 cm/s. With respect to the relatively weak 'background circulation' of 2.5 cm/s, these values indicate a fluctuating acceleration by a factor of about three. So, the travel time of one complete 'cycle' around the whole 220m-depth contour would be reduced rhythmically to be about 20 days.

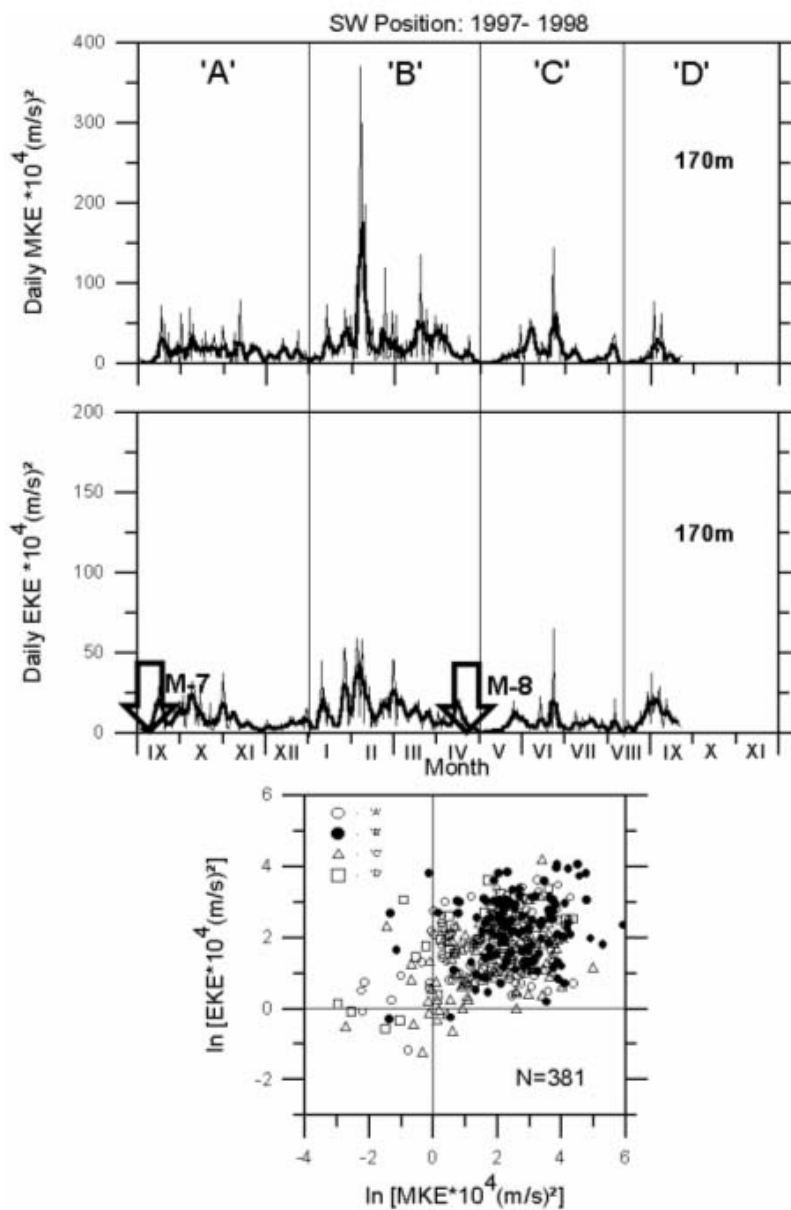


Fig.12 b) N= 381 days at the SW position (57°04.53'N, 19°45.12'E).

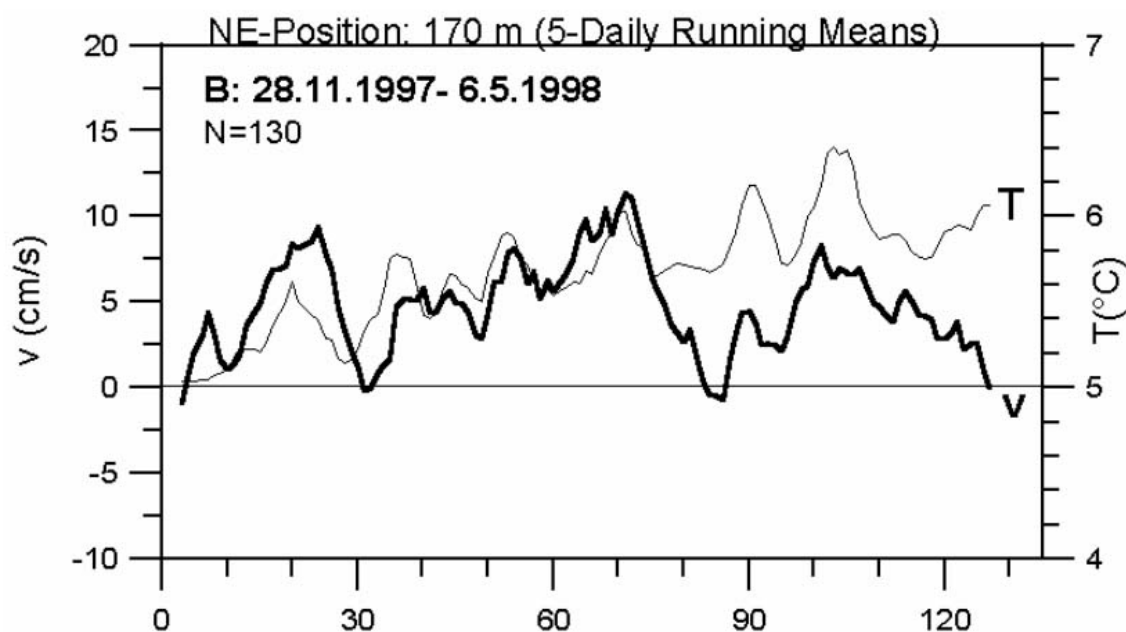


Fig.13 Five daily running means of temperature (T) (thin line) and meridional current component (v) (bold line) for N= 130 days of the inflow period (B) at 170m depth of the NE position.

4. Snapshot Mass Field Patterns

In temporal vicinity of the detected wintry inflow of dense deep water into the EGB, the monitoring programme of the IOW carried out hydrographic measurements along the line of steepest descent in the bottom topography. The selected section starts with station BMP K5 (113) in the south-west and ends with station 286 (Baltic Year station BY 20A) in the north-east. Its course is depicted in Fig.1. In the Baltic Sea, salinity essentially determines density. Therefore, vertical plots of the salinity distribution well describe the propagation of dense deep water by regional peak values. Resulting transects are shown above a rough bathymetry in Fig.14. Concerning the deep inflow towards the EGB, the upper panel describes pre-inflow conditions measured during October 24 until November 5, 1997. Salty deep water ($S > 18$ psu) filled up deepest parts of the Arkona Basin (AB) and those of the Bornholm Basin (BB) ($S > 16$ psu). It reached the Bornholm Basin during the end of October 1997. That means the inflow signal needed at least four weeks to overcome the distance of about 230 km between the Darss Sill and

the central Bornholm Basin. Consequently, the mean velocity of eastward spreading deep water was about 9 cm/s. This value confirms the mean propagation speed of 11 cm/s between the Darss Sill and the EGB. Accepting this value for a farther eastward propagation of saline deep water along this section, the associated increase in both salinity and temperature should be measured during the end of November or the beginning December 1997 in the central EGB, as it is demonstrated by abruptly increasing temperatures in Fig. (9, 10).

Thus, relatively dense water ($S > 14$ psu) overwhelmed the sill at the entry into the Stolpe Furrow (SF). However, saline near bottom water with $S > 12$ psu could not be observed above the steep topographic slope forming the transition area between the exit of the SF and the entry of the EGB. The upper panel shows that water of comparable salinities only filled up deepest parts ($P > 190$ dbar) of that basin. The situation had essentially changed four months later. The transect, which was carried during February 6-20 1998, describes the middle phase of the identified inflow. In the meantime, the inflow into the EGB lifted the level of the 12 psu isohaline to about 170 dbar. Again, no dense bottom water with $S > 12$ psu was detected in the transition area between the SF and the EGB. The vertical thickness of the layer with dense deep water significantly decreased not only in the Stolpe Furrow but also in both the Bornholm Basin (BB) and the Arkona Basin (AB). During the following three months, the situation had not changed dramatically in western Baltic basins. This follows from the transect plotted in the bottom panel. It was carried out in May 4-13, 1998. In the EGB, the lifting of the 12 psu isohaline continued and reached about 150 dbar. Again, no saline deep water could be observed between the exit of the SF and the entry of the EGB. This suggests two possibilities: Either

- (i) inflow events occurred occasionally during relatively short time episodes, or
- (ii) BMP monitoring stations do not follow the path way of deep water intrusions.

In the case (i), dense deep water overcomes the sill at the exit of the SF to propagate towards the EGB sporadically. All three snapshots of vertical salinity distributions, which result from the monitoring programme, could not resolve the temporal nature of that inflow properly. Case (ii) takes into account the observational fact that the inflow signal was firstly observed at the NE position and somewhat later at the SW position. Under the influence of the deflecting Coriolis force, the inflow event probably followed the eastern topographic flank towards the EGB and not the line of steepest descent in the bottom topography. Therefore, BMP monitoring stations did not resolve spatially the path way of that inflow. However, there is no question that an inflow event happened in the mean time. The upward displacement of the 12 psu surface well indicated the changed net volume of dense deep water within deepest parts of the EGB.

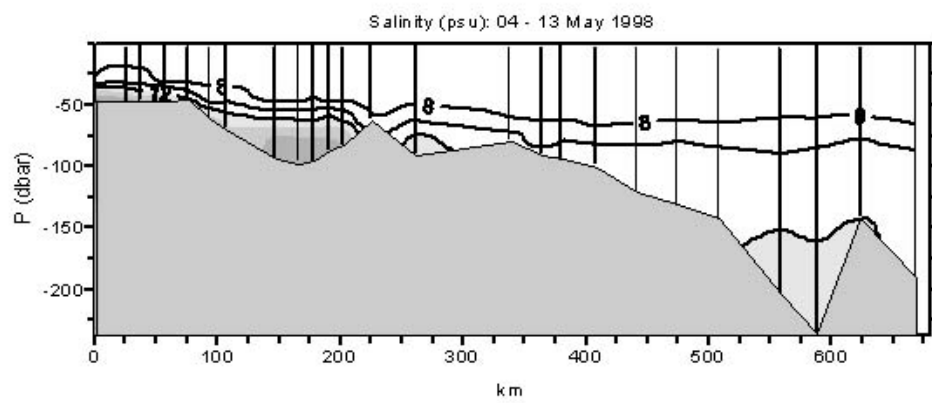
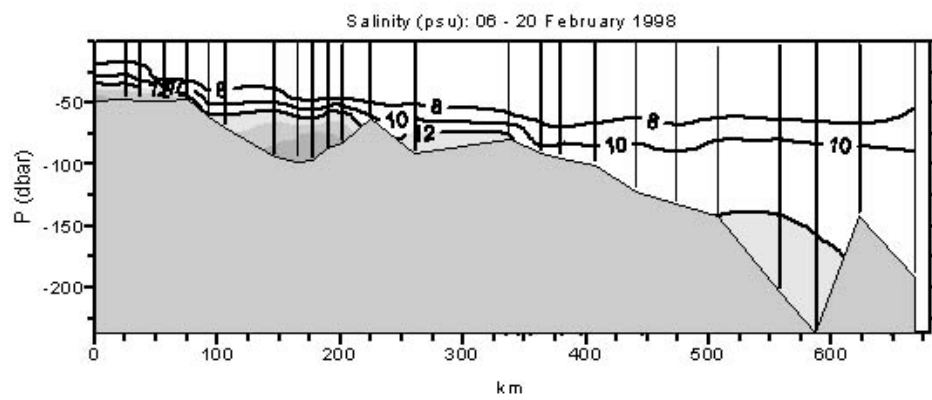
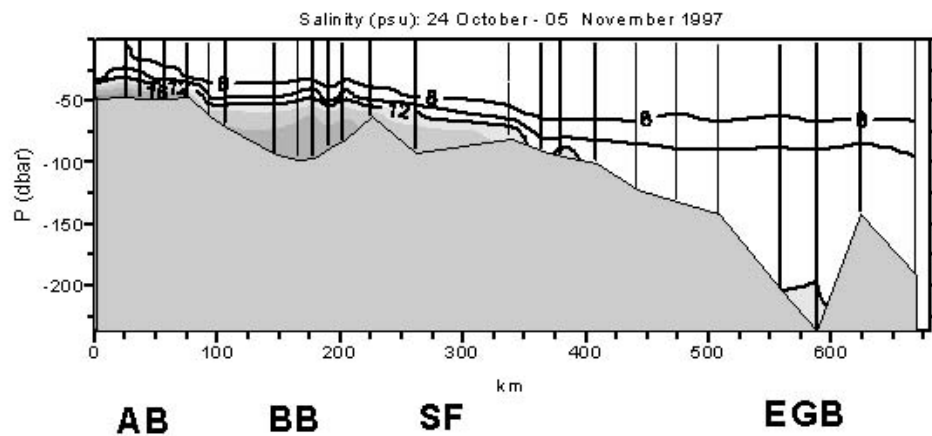


Fig.14 Vertical salinity distributions along the line (km) of steepest descent in the water depth resulting from three cruises of the IOW (Baltic Monitoring Programme) over a rough bottom topography; station position are shown in Fig.1; the transect starts with station 113 in the Arkona Basin (AB), it crosses both the Bornholm Basin (BB) and the Stolpe Furrow (SF) to end at station 286 in the north of the Eastern Gotland Basin (EGB); concerning the EGB, the upper panel characterises pre-inflow conditions in October/ November 1997; the middle panel points to the inflow period of dense deep water, which was well developed in February 1998 while the lower panel indicates the post-inflow situation in May 1998; the bold line shows the 12 psu isohaline; near bottom layers of higher salinity are differently stippled.

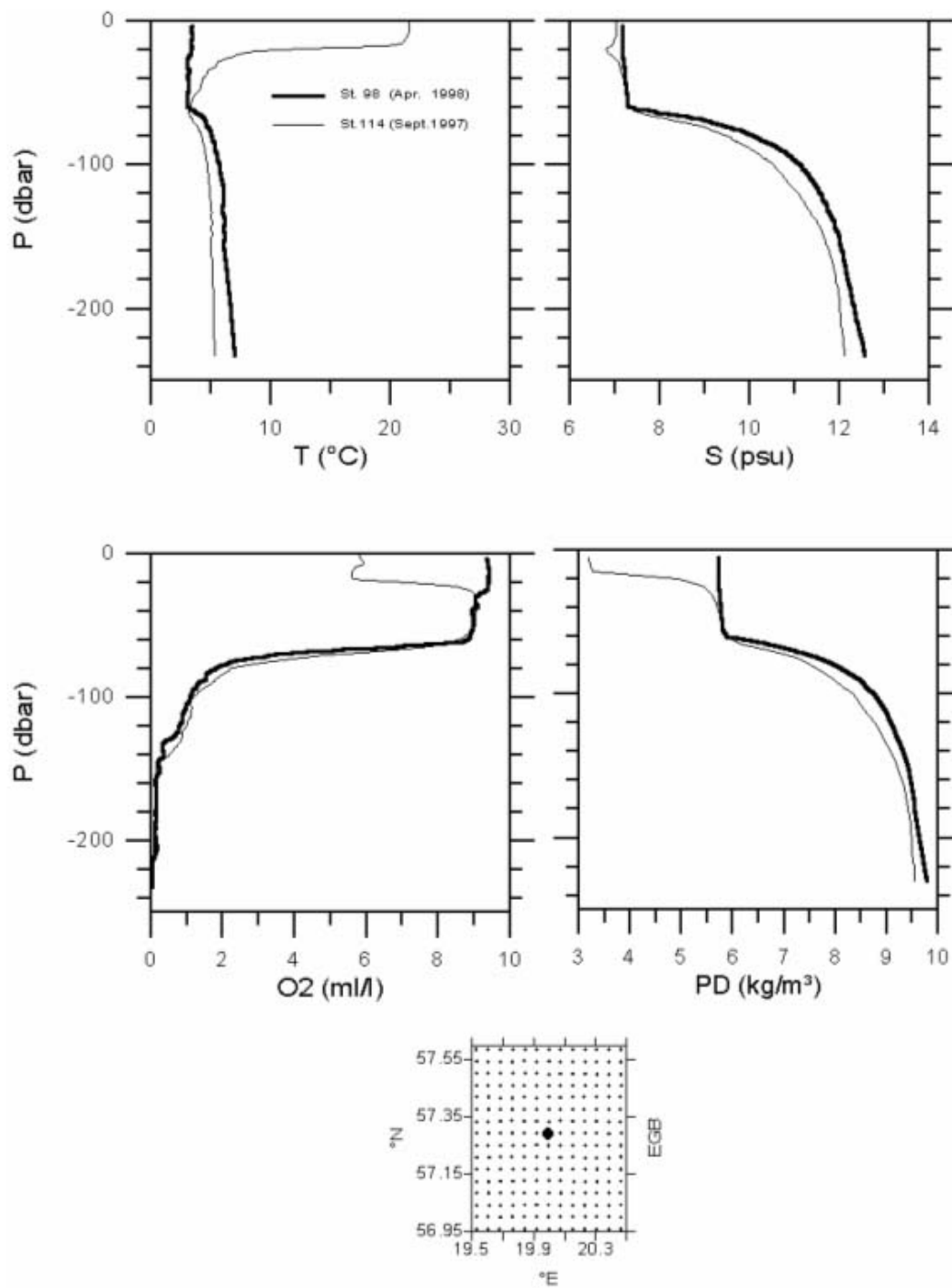


Fig.15 Vertical profiles of temperature (T), salinity (S), dissolved oxygen (O_2), and potential density (PD) in the central Eastern Gotland Basin (EGB) measured at station 114 in September 1997 (thin line) and at station 98 in April 1998 (bold line) during two MESODYN campaigns; station's position is separately indicated and locates in vicinity of station 271 (BY15A) of the Baltic Monitoring Programme.

Mass-field patterns were measured by the MESODYN-7 campaign (M-7) from August 29 until September 4, 1997, as well as by the MESODYN-8 survey (M-8) carried out during April 19-24, 1998. The campaign M-7 surveyed pre-inflow conditions (A) while that of M-8 was carried out during the post-inflow period (C). The observational time of both cruises is given by arrows in Fig.9, Fig.10, and Fig.12. Differences in the vertical structure of the mass field are shown by profiles of temperature, salinity, dissolved oxygen, and potential density in Fig.15. The selected position lies in the central part of the basin, immediately in vicinity of the central BMP station 271 (BY15A). Layers deeper than the pressure level of 80 dbar elucidate increasing temperatures, salinities and potential densities without a significant improvement in the oxygen conditions.

Zonal transects, which involve this central station, depict vertical structures of the potential density (PD) in the range in between 9 kg/m^3 and 9.5 kg/m^3 in Fig.16. In the following we use the anomaly $\text{PD} = 9.3 \text{ kg/m}^3$ instead of the potential density $\text{PD} = 1009.3 \text{ kg/m}^3$. Thin lines show the late summer situation, which characterises pre-inflow conditions (A) in the early September, 1997. Pressure levels of all selected isopycnals reveal a concave shape. Such curvature coincides with a geostrophically adjusted anticyclonic (clockwise) circulation. In comparison, bold lines represent those of the post-inflow situation (B) observed in April, 1998. This situation elucidates a convex shape of isopycnal surfaces with a doming above the eastern topographic flank of the basin. This doming suggests geostrophic motions, which rotate anticlockwise around topographic contours. Different relative dynamical topographies (not shown) confirm this tendency. Squashed isopycnals of the situation (B) indirectly indicate an outbreak of deep water by the upward displacement of dense isopycnal surfaces over the eastern flank of the EGB. For instance, the mean pressure level of $\text{PD} = 9.5 \text{ kg/m}^3$ was about 200 dbar during the pre-inflow situation but 170 dbar during the post-inflow period. Such changed pressure levels of deep isopycnals permit the estimation of mean vertical velocities as well as changes in participating volumes of dense deep water in reaction on the net inflow.

5. Changed Deep Volumes

In the EGB, the target area of the project MESODYN covers 3945 km^2 . Its total volume is 682 km^3 . In order to estimate changed volumes of dense deep water we focus attention on selected isopycnal surfaces sealing closed bathymetric contours beneath 190 m depth (190 dbar). We got a linear area (A) - depth (D) relationship by triangulation of the bathymetric map shown in Fig.2.

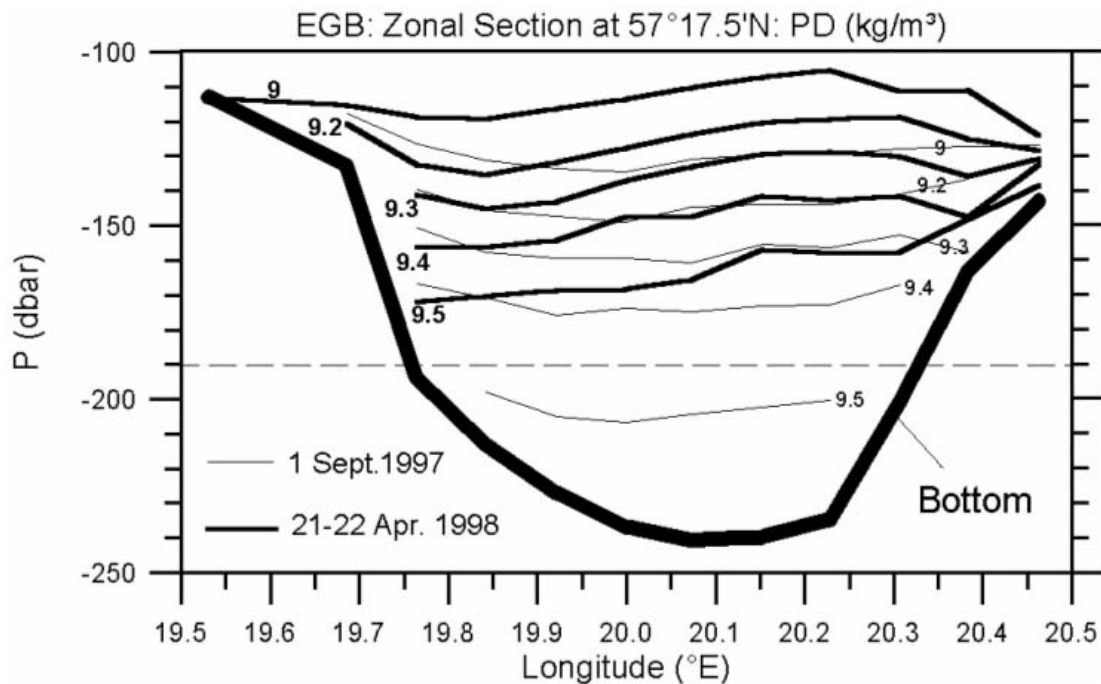


Fig.16 Pressure levels of deep potential density surfaces along a zonal section at $57^{\circ}17.5'N$ between $19^{\circ}32.1'E$ and $20^{\circ}27.9'E$ through the Eastern Gotland Basin during September 1997 (thin lines) and during April 1998 (bold lines); closed bathymetric contours are bounded by the 190m isobath (dashed line).

The maximum depth of 241.8 m was chosen to be zero. Areas of upper horizons were determined by 26 steps of $\Delta D = 2$ m. The resulting regression is $A_M (\text{km}^2) = 28.16641 * D(\text{m})$ within the interval $[0 \leq \Delta \leq 52]$ m. It provides the determination coefficient $R^2 = 0.999$. The index (M) refers to MESODYN's topographic data set. The resulting curve is plotted in Fig.17. For example, this regression estimates $A_M = 1465 \text{ km}^2$ for $D = 52$ m while the triangulation provides 1467 km^2 for the 190 m isobath. Using the Kriging method of the SURFER program (Golden Software) this area is calculated to be 1404 km^2 . The difference between both estimations is smaller than 4%. Beneath 190 m depth, the SURFER program calculated the total volume of $V = 37 \text{ km}^3$ while the regression volume is $V_M = 38 \text{ km}^3$. In this case, the resulting difference is smaller than 2% and probably based on numerical uncertainties. Finally, the related volume-depth regression exhibits a parabolic shape by $V_M (\text{km}^3) = 0.0140832 * D^2(\text{m})$.

Pressure levels of selected potential density surfaces have been compared to obtain an information about the volume of injected dense water. No isopycnal surface could be identified, which was present in both situations beneath the level of $p = 190$ dbar. That means the whole old deep water with a volume of about 38 km^3 was, at least, replaced by the inflow of denser water. At the NE position, the inflow period lasted 130 days. Consequently, the minimum in the mean volume transport was about $0.3 \text{ km}^3/\text{d}$. To estimate a more precise value we choose the density surface of $PD = 9.7 \text{ kg/m}^3$, which was absent in the deep EGB during September, 1997.

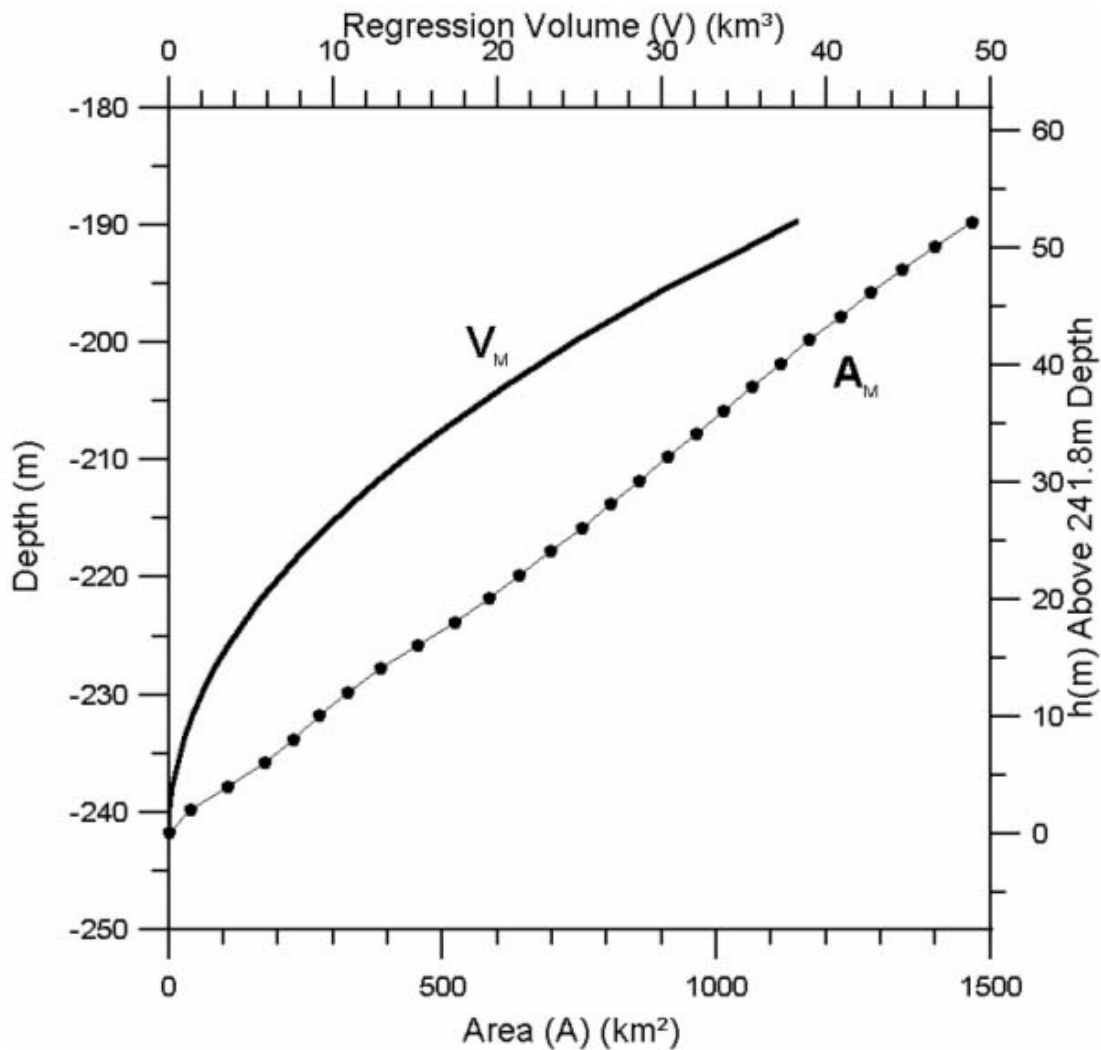


Fig.17 Regression volume (V_M) resulting from the area (A_M) – depth (m) relationship of the MESODYN topography as derived for horizons deeper than 190 m; the area A_M results from triangulation in steps of two metres (dots) above the maximum depth of 141.8 m (right ordinate).

Here, we take into consideration that an unknown amount of dense water should be streamed out above isobaths shallower than 190 m depth. Assuming closed vertical borders of the MESODYN-area for pre- and post-inflow conditions, we computed volume differences between the PD surfaces of 9.4 and 9.45, 9.45 and 9.5, as well as those between 9.5 and 9.55 kg/m^3 . It resulted the constant change in volume of $\Delta V = +56 \text{ km}^3$ for each of the three enclosed sub-layers. This constant value suggests that the volume balance was well equalised between the deep inflow and the upper outflow. Thus, the related mean volume transport into the deep EGB was estimated to be about $0.4 \text{ km}^3/\text{d}$. In April 1998, the spatially averaged pressure level of $p(\text{PD}=9.7)$ was $(208 \pm 8) \text{ dbar}$. Accepting that $\Delta p=1 \text{ dbar}$ roughly corresponds to $\Delta D = 1 \text{ m}$, it results $\Delta V = (16 \pm 1) \text{ km}^3$ via the

mentioned regression. The SURFER program computed $\Delta V = 20 \text{ km}^3$ between this density surface and the sea bed. Independently of the numerical method used, we like to conclude that about 18 km^3 water, which was denser than 9.7 kg/m^3 , filled about half the available volume by a volume transport of about $0.14 \text{ km}^3/\text{d}$. This value contributes to about 50% of the volume transport needed to replace the entire water within the volume of closed bathymetric contours.

Due to mean upward motions, density layers revealed a squeezing between the pre-inflow and the post-inflow situation. Independently of the volume capacity of the deepest part of the basin, such shrinking processes of the layer thickness must be caused by upward displacements of deepest isopycnal surfaces. This is confirmed by spatially averaged shrinking values ranging from -5 dbar ($9.4 \leq \text{PD} \leq 9.45$) kg/m^3 to -13 dbar ($9.5 \leq \text{PD} \leq 9.55$) kg/m^3 . Thus, related upward motions decreased towards less dense sub-layers. The vertical profile of the spatially averaged vertical velocity $\langle w \rangle$ is drawn in Fig. 18. Its confidence range increases to denser PD's due to decreasing station numbers. This plot exhibits a parabolic shape like that of vertical changes in the deep topographic volume (Fig.17). Considering spatial patterns of $\langle w \rangle$ for selected sub-layer, all isotaches well reflect contours of the deep bottom topography. An example is plotted above the rough bathymetry in Fig.19. The centre of peak values in upward motions coincides with the topographic centre of the EGB. In summary, there is some observational evidence that such deep upward velocities vertically integrate corresponding changes in the deep topographic volume.

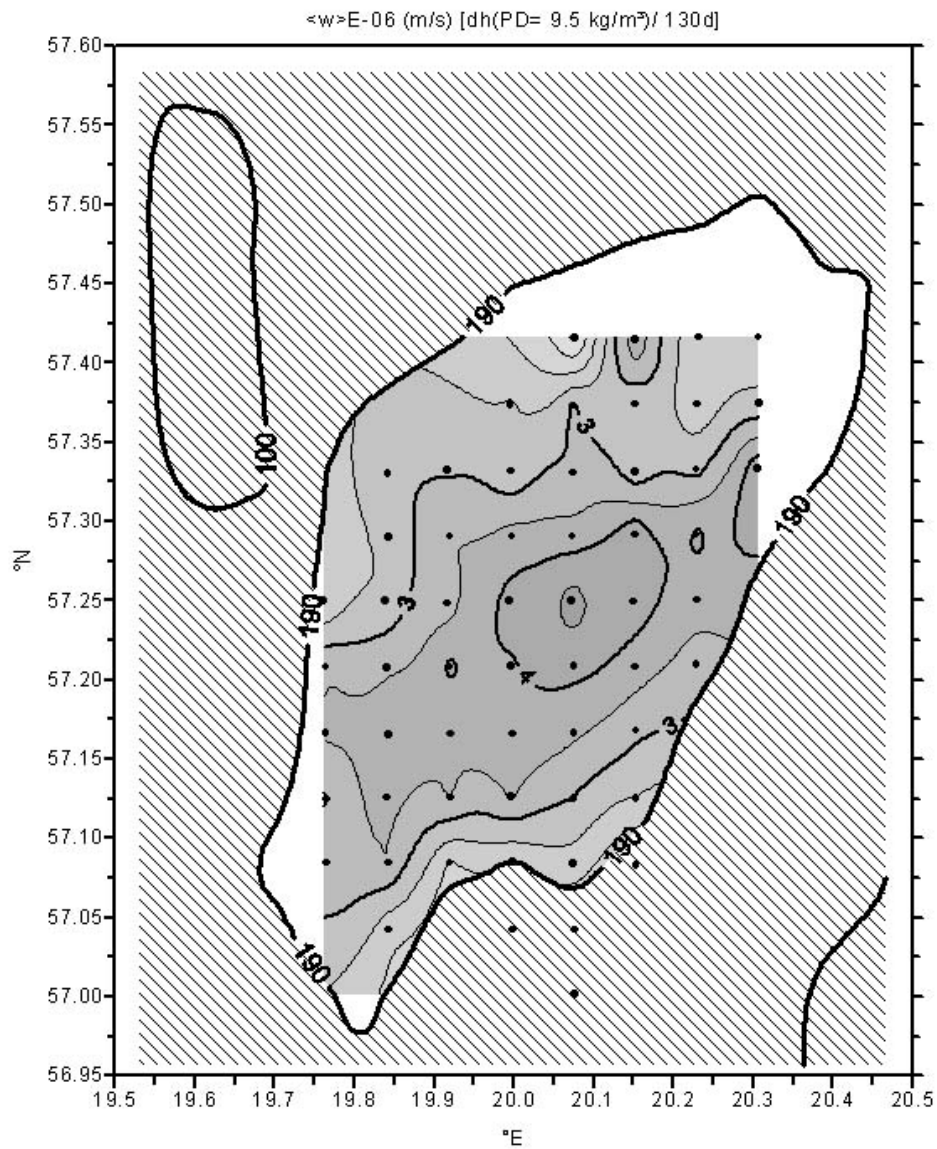


Fig.18 Vertical profile of the mean vertical velocity $\langle w \rangle$ estimated from the spatially averaged upward displacement (dh) of six PD-surfaces between the campaigns of M7 (pre-inflow situation) and M8 (post-inflow situation) with a time difference of 130 days; error bars describe the 95% significance level according to the t -distribution; the related number of stations increases with decreasing density.

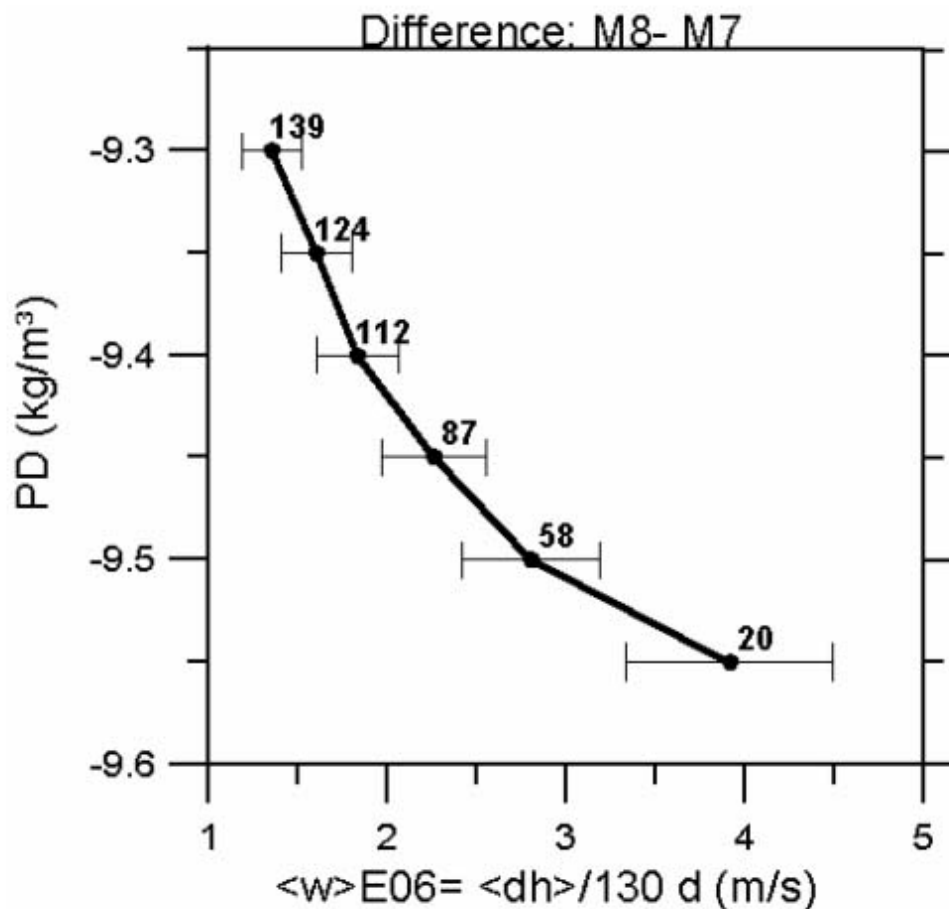


Fig.19 Spatial patterns of the mean vertical velocity $\langle w \rangle$ as in Fig. 18 but for the isopycnal surface $PD = 9.5 \text{ kg/m}^3$; station positions (dots) are roughly bounded by the 190 m isobath; the 100 m depth contour indicates shallower areas of the Klints Bank; note that the dosed $4 \cdot 10^{-6} \text{ m/s}$ -isotache is found immediately above the deepest part of the basin.

6. Summary and Conclusions

According to MATTHÄUS et al. (1998) there was an extremely warm summer in 1997. Two storms in September and the beginning October transported exceptionally warm and saline water across topographic sills into deep Baltic basins. Comparing changes in the sea level at station Landsort (Baltic Proper) with those of differences between stations Viken (south Kattegat) and Klagshamn (south-west Baltic Sea), the net flow through Danish straits into the Baltic Sea was estimated to be about 138 km^3 with a mean volume transport of about $10 \text{ km}^3/\text{d}$ during the early September, 1997. About a quarter of that inflow passed the Sound, BROMAN (1999, personal communication). In comparison, the volume flux through the Sound was smaller (1/7) during January 1993, JACOBSEN (1995). Comparing both values, the inflow event of the 'late winter - early spring type' (January 1993) involved smaller transports passing the Sound than that of the 'late autumn - early winter type' (September 1997). The last inflow lasted about 14 days. This

value confirms previous estimations of the literature and exceeds the critical through flow time of Danish straits by the factor of about 1.5. This was an essential precondition for the effective inflow event, which started to pass the Darss Sill on September 18, 1997. It was accompanied by eastward blowing winds as well as by eastward directed currents covering the whole water column. The associated inflow event pushed relatively warm ($T > 15^{\circ}\text{C}$) but saline water ($S > 17$ psu) eastward across the Darss Sill. It led to positive temperature anomalies of 3 - 4 K in the deep Bornholm Basin, which was filled with water of salinities larger than 15 psu. Water with properties between $(9-11)^{\circ}\text{C}$ and $(14-15)$ psu passed the Stolpe Furrow at the end of October, MATTHÄUS et al. (1998). Thereafter, the inflow signal propagated towards the Eastern Gotland Basin (EGB). Here, 'new deep water' replaced properties of 'old deep water' within layers beneath the perennial pycnocline during the December 1997. This process lasted until April 1998. Temperatures of deep layers significantly increased from about 5°C to about 6°C . Sporadically occurring maximum temperatures were insignificantly smaller than reported from the historical peak value of about 7°C during the winter 1976.

Following the path-way of steepest descent in the sea bed, the distance between the exit of the Stolpe Furrow and the NE mooring was about 240 km. The spreading of warm but dense deep water needed at least 30 days to overcome this distance. The associated minimum speed in the mean north-eastward propagation was estimated to be about 10 cm/s. This value confirms the minimum velocity of eastward spreading deep water between the Darss Sill and the Stolpe Furrow in the western Baltic Sea. However, our observations suggest that the real inflow event probably did not follow the line of steepest descent in the sea bed between the exit of the Stolpe Furrow and the entry in the EGB. Probably rhythmically triggered inflow events sporadically propagated with temporally intensified current velocities along the eastern topographic flank towards the EGB. Associated velocities must be somewhat larger than the estimated propagation speed of about 10 cm/s.

For the first time, half hourly and hourly sampled temperature series with lengths between 326 days and 436 days well documented the inflow of warm but dense deep water at two positions in north-east (NE) and south-west (SW) of the EGB during the winter 1997/98. Moored current meters continuously recorded the motion field at 170 m depth beneath the perennial pycnocline. Both strings were anchored at 220 m water depth above topographic flanks of the EGB. Resulting time series reveal a mean cyclonic circulation of about 2.5 cm/s. Its direction followed deep bathymetric contours and pointed into the north-west sector at the NE position but into the south-east sector at the SW position. This cyclonic circulation lasted longer than one year. Such a deep water rotation was earlier observed by current measurements with a total length of several weeks by DIETRICH and SCHOTT (1974) and MITTELSTAEDT (1996). Therefore, it seems to be that anticlockwise motions with velocities between 1 and 3 cm/s determine the deep circulation in the EGB for long time periods, which exceed one complete seasonal cycle.

Hydrographic data of the monitoring programme and two hydrographic surveys with an eddy-resolving station grid provided snapshots in mass field patterns to characterise related pre-inflow and post-inflow situations. These MESODYN field campaigns used a regular station spacing of 4.6 km, which sufficiently resolved the first mode of the baroclinic radius of deformation. This scale describes characteristic spatial patterns of motions affected by stratification. Its spatially averaged mean was 9 km (September 1997) and 7 km (April 1998). Detected vertical displacements of deep isopycnal surfaces between pre- inflow and post-inflow situation enabled to estimate the net volume of replaced dense water. The changed volume between selected isopycnals and the sea bed was determined by numerical triangulation of the echo-sounded topography. Released mean vertical velocities in the order of 10^{-6} m/s decreased with decreasing water depth and well reflected related changes in the bathymetric volume of the deep EGB.

The inflow of at least 56 km³ warm, saline, but weakly oxygenated deep water started above the eastern flank of the basin. That means about 40% of the net flow through the Danish straits at the entry into the Baltic Sea filled up deep parts of the EGB with a delay of about three months. The renewed volume of deep water lies in the order of monthly fresh water supply reported by BROGMUS (1952). Concerning the area under investigation, the water balance requires a previous outflow of near surface water of the same order. The related volume transport was about 0.5 km³/d. This magnitude was also observed by RYDBERG (1978). He estimated volume transports between 0.4 and 3 km³/d for saline deep water ($S > 10.5$ psu) crossing the Stolpe Furrow towards the EGB. Here, the isobath of 190 m depth 'seals' deepest parts of the basin. Beneath this water depth, the resulting volume capacity is about 38 km³. Half of that volume was filled by water denser than 1009.7 kg/m³ in winter 1997/98.

The whole inflow period of about 130 days was accompanied by a linear trend of increasing temperatures within layers between 170 m and 140 m depth locating below the permanent pycnocline over topographic flanks of the deep basin. At the NE position, this trend started at the nearly constant level of about 5°C at the end of the pre-inflow period (28 November 1997) and ended at the nearly constant level of about 6°C at the end of the inflow period (6 May 1998). Such a warming confirms a net inflow of the 'late autumn - early winter type'. Consequently, deep isopycnal surfaces were displaced upward to produce a doming above the basin's centre. The responsible cyclonic deep circulation maintained this doming until the post-inflow situation.

The inflow situation was accompanied by intensified rotation velocities within deep layers of the EGB. Mean speeds accelerated by a factor of about two up to three. During that time period, a linear relationship could be detected between logarithmic values of the daily averaged mean kinetic energy and those of the daily eddy kinetic energy at the NE position. Such a correlation could not be detected at the SW position and also not for both the pre-inflow and post-inflow situation at the NE position. Consequently, energetic fluxes from the low frequency range into the high frequency range of the motion field dominated in the source area of the inflow. High frequency fluctuations of the current regime point to periods, which are somewhat shorter than the daily cycle. According to HOLLAN (1969), it can be expected that most of the resulting energy accumulation concentrates on periods in vicinity of the local inertial period of about 14.2 hours. The role of inertial motions with respect to any mixing processes is still unclear. However, there is some observational evidence that near-inertial waves and the vertical current shear can release intense mixing locally. For instance, LILOVER et al. (1988) reported a vertical propagation of such waves in the Bornholm Basin from current measurements. They concluded that breaking internal waves with a near inertial period may create patches by hydrodynamic instabilities, which could be responsible for locally intensified mixing plumes.

At the SW position, a shallow cold water event was observed within layers between 170 m and 140 m depth. It lasted about three weeks and was accompanied by a significant intensification of both the daily mean kinetic energy and the daily eddy kinetic energy. According to ELKEN et al. (1988), such phenomena play an important role in lateral and vertical mixing within layers above the level of 140 dbar in the EGB. Such features possess diameters of several kilometres. Their thickness commonly exceeds several decametres. Analysing T-S curves, they demonstrated that such intrusions originate from the near-slope region. Released temporal fluctuations of the thermal field also indicated quasi-periods of about 20-22 days. Visually, six peak values were superimposed on the linearly increasing temperature trend observed at both moored strings during the inflow period of 130 days. Such low frequency fluctuations were associated with patterned structures in the mass field with diameters twice of the radius of deformation. By analysing time series of sea level data, SAMUELSSON and STIGEBRANDT (1996) concluded that wind-produced dynamics dominate all circulation patterns in the Baltic Sea on time scales shorter than about one month. In order to get a hint about the origin of such 20 day fluctuations, we additionally analysed daily winds and daily differences in the air pressure observed at different

stations in vicinity of the EGB during the inflow period. Results are objective for further studies and not shown here. However, power spectra of zonal winds show a significant accumulation of energy for periods of about 20 days.

Two weeks lasting westerly winds produced eastward flowing currents in shallow water regions near the Darss Sill in the south-west Baltic Sea. Opposite conditions can be expected in deep Baltic basins locating farther in the east. According to KRAUSS and BRÜGGE (1991), the deep layer flow increases in contra-direction to the wind due to sea level inclinations in response to the wind forcing. The working hypothesis rose up that changed wind directions, which temporally influenced much larger spatial scales, could be responsible for significant anomalies in sea level. Relatively low frequency changes in the forcing conditions probably released rhythmically modified internal pressure gradients and caused pulsating inflow events, which overwhelmed the sill at the exit of the Stolpe Furrow. Following the steep topographic slope in the transition area between the Stolpe Furrow and the Eastern Gotland Basin, triggered overflows sporadically intensified the deep cyclonic circulation above the eastern topographic flank of the EGB. The analysed data sets suggest the following scenario:

The first rotation cycle of relatively warm but dense deep water needed about 60 days to travel around the contour of the 220 m isobath with a length of about 130 km. It abruptly started above the eastern topographic flank of the basin (NE position) during the end of November 1997 to form a rotating wedge-shaped frontal zone following closed bathymetric contours. Internally established pressure gradients between the basin's centre (light 'old water') and neighbouring rims (heavy 'new water') accelerated the anticlockwise rotation around the basin. Such pressure gradients between the basin's centre (low pressure) and neighbouring topographical flanks (high pressure) balance the geostrophic part of the deep water rotation. Once deepest parts of the basin were filled up by dense 'new water', subsequent intrusions lifted upper layers with lighter water upwards. Associated vertical velocities indicated the order of 10^{-5} m/s. For instance, a mean vertical velocity of $1.7 * 10^{-5}$ m/s is capable to fill parts of the basin deeper than 190 m during 130 days. Mixing processes, which were released in the wake of this frontal zone, temporally and spatially merged properties of 'young deep water' with those of 'old deep water' as well as with those of upper layers. Consequently, both internal pressure gradients and associated rotation speeds decreased. The next pulse of injected dense water again strengthened radial pressure gradients. The rotation velocity accelerated to daily mean values to be in the range between 5 and 10 cm/s. Each following rotation cycle followed elliptic contours of the bottom topography. It started with peak values in its orbital velocity and a maximum in temperature at the thermal level, which was produced by mixing and upward lifting of isopycnal surfaces in the wake of previous rotation cycles. So, the detected linear temperature trend can be explained if the amount of injected dense water was of the same order for each rhythmically occurring inflow event and if processes of adjacent mixing were of comparable intensity. After the last inflow pulse, remaining mixing reduced pressure gradients between the centre of the basin and neighbouring topographic flanks to aspire a state of stationary equilibrium. Finally, the anticlockwise deep rotation relaxed to values of the 'background circulation' with velocities of about 1 – 3 cm/s. Therefore, the identified inflow period (B) with a duration of 130 days was characterised by a sequence of six rhythmically occurring inflow events with a mean duration of about 22 days. Their origin probably lies in corresponding fluctuations of westerly winds affecting barotropic and baroclinic pressure gradients, which affect the whole basin scale.

In the Baltic Sea, the EGB reveals the largest volume capacity to store dense deep water for a certain time. This way, it plays a key role with respect to processes of water transformation for the whole Baltic Proper. The volume capacity of deep basins essentially determines residence times of dense water and exchange rates for water mass transformation acting on different temporal scales. Concerning the volume transports discussed, another topographic volume capacity would provide other exchange rates of deep water. In comparison to the MESODYN

bathymetric map of the EGB, the bottom topography proposed by SEIFERT and KAYSER (1995) underestimates the volume beneath 190 m depth by about 45%. This example shows that coarse bottom topographies, which are frequently used in numerical circulation models, probably overestimate net rates of the deep water exchange. Associated residence times must be somewhat too short. Without improved topographic maps of the Baltic Sea, such approaches permanently involve an error source. We urgently need exact topographic data for all deep Baltic basins in context with internationally co-ordinated field campaigns, which include eddy resolving hydrographic surveys as well as long time series, to understand qualitatively and quantitatively the consequence of such inflow events for the Baltic ecosystem.

Acknowledgement

This study attributes to the German hydrographic programme 'Meso-scale Dynamics (MESODYN)' of the Russian-German project 'Research in the Baltic Sea' supported by the Ministry of Science and Technical Politics of the Russian Federation and the Ministry of Education and Scientific Research of the Federal Republic of Germany; we gratefully acknowledge all supports provided by crews and officers of both research vessels of the IOW 'A. v. Humboldt' and 'Prof. A. Penck' as well as the submission of Swedish sea level data by B. Broman of the Swedish Meteorological and Hydrological Institute; series of Arkona winds were kindly provided by the German Meteorological Service while discussions with W. Matthäus prompted us to take care on specific Baltic problems.

References

- BÖRNGEN, M., 1978: On the causes of the strong salt inflows into the Baltic. In: Proceedings of the 11th Conference of the Baltic Oceanographers, Rostock, 305-315.
- BROGMUS, W., 1952: Eine Revision des Wasserhaushaltes der Ostsee. Kieler Meeresforschung, **9**, 15-42.
- DIETRICH, G., 1950: Die natürlichen Regionen von Nord- und Ostsee auf hydrographischer Grundlage. Kieler Meeresforschungen, **7**, 35-68.
- DIETRICH, G., SCHOTT, F., 1974: Wasserhaushalt und Strömungen. In, L. Maggaard and G. Rheinheimer (Editors), Meereskunde der Ostsee. Springer-Verlag, Berlin, Heidelberg, New York, 33-41.
- ELKEN, J., PAJUSTE, M., KOUTS, T., 1988: On intrusive lenses and their role in mixing in the Baltic deep layers. In: Proceedings of the 16th Conference of the Baltic Oceanographers, Institute of Marine Research Kiel, Kiel, 367-376.
- FENNEL, W., SEIFERT, T., KAYSER, B., 1991: Rossby radii and phase speeds in the Baltic Sea. Continental Shelf Research, **11**, 23-36.
- HELCOM, 1986: Water balance of the Baltic Sea. Baltic Sea Environmental Proceedings, Vol.16, 1-174.
- HOLLAN, E., 1969: Die Veränderlichkeit der Strömungsverteilung im Gotland-Becken am Beispiel von Strömungsmessungen im Gotland-Tief. Kieler Meeresforschungen, **25**, 19-70.
- JAKOBSEN, F., 1995: The major inflow to the Baltic Sea during January 1993. Journal of Marine Systems, **6**, 227-240.
- KALLE, K., 1943: Die große Wasserumschichtung im Gotland-Tief vom Jahre 1933/34. Annalen der Hydrographie und maritimen Meteorologie, **71**, 142-146.
- KOUTS, T. OMSTEDT, A., 1993: Deep water exchange in the Baltic Proper. Tellus, **45**(A), 311-324.
- KRAUSS, W., BRÜGGE, B., 1991: Wind-produced water exchange between the deep basins of the Baltic Sea. Journal of Physical Oceanography, **21**, 273-384.
- KRÜGER, S., 1997: Meeresmeßtechnik im Institut für Ostseeforschung Warnemünde. Deutsche Gesellschaft für Meeresforschung, **3**, 23-29.
- LARSEN, B., KÖGLER, F. C., 1975: A submarine channel between the deepest parts of the Arkona and the Bornholm basins in the Baltic Sea. Deutsche Hydrographische Zeitschrift, **28**, 274-276.
- LASS, H. U., 1988: A theoretical study of the barotropic water exchange between the North Sea and the Baltic and the sea level variations of the Baltic. Beiträge zur Meereskunde, (H.58), 19-33.
- LASS, H.U., MATTHÄUS, W., 1996: On temporal wind variations forcing salt water inflows into the Baltic Sea. Tellus, **48**(A), 663-671.

- LASS, H. U., R. SCHWABE, R., 1990: An analysis of the Salt Water Inflow into the Baltic in 1975 to 1976. *Deutsche Hydrographische Zeitschrift*, **43**, 97-125.
- LILOVER, M. J., OTSMANN, M., TAMSALU, R., 1988: Near-inertial waves and shear instability. In: *Proceedings of the 16th Conference of the Baltic Oceanographers*. Institut of Marine Research Kiel, Kiel, 648-652.
- MATTHÄUS, W., 1984: Climatic and seasonal variability of oceanological parameters in the Baltic Sea. *Beiträge zur Meereskunde*, (H. 51), 29-49.
- MATTHÄUS, W., FRANCK, H., 1992: Characteristics of major Baltic inflows- a statistical analysis. *Continental Shelf Research*, **12**, 1375-1400.
- MATTHÄUS, W., LASS, H. U. 1995: The recent salt inflow into the Baltic Sea. *Journal of Physical Oceanography*, **25**, 280-286.
- MATTHÄUS, W., NAUSCH, G., LASS, H. U. , NAGEL, K., SIEGEL, H., 1998: The Baltic Sea in 1997- impacts of the extremely warm summer and of the exceptional Oder flood. *Deutsche Hydrographische Zeitschrift*, **50**, 47-69.
- MITTELSTAEDT, E., 1996: The subsurface circulation in the Gotland Deep. In: E. Hagen (Editor), *GOBEX- Summary Report*. Meereswissenschaftliche Berichte, No.19. Institut für Ostseeforschung Warnemünde, 20-23.
- MOHRHOLZ, V., 1998: Transport- und Vermischungsprozesse in der Pommerschen Bucht. *Meereswissenschaftliche Berichte*, No. 33, Institut für Ostseeforschung Warnemünde, 106 pp.
- NEHRING, D., FRANCKE, E., 1981: *Hydrographische Untersuchungen in der Ostsee von 1969-1978*. Geodätische und Geophysikalische Veröffentlichungen, R.IV, H.35, 220 pp.
- OMSTEDT, A., AXELL, L. B., 1998: Modelling the seasonal, interannual, and long-term variations of salinity and temperature in the Baltic proper. *Tellus*, **50(A)**, 637-652.
- REISSMANN, J., 1999: Bathymetry of four deep Baltic basins. *Deutsche Hydrographische Zeitschrift*, **51**, 489-497.
- RYDBERG, L., 1978: Deep water flow and oxygen consumption within the Baltic. *Göteborgs Universitet Oceanografiska Institutionen*, Göteborg, No.27, 12 pp.
- SAMUELSSON, M., STIGEBRANDT, A., 1996: Main characteristics of long-term sea level variability in the Baltic sea. *Tellus*, **48(A)**, 672-683.
- SCHINKE, H., MATTHÄUS, W., 1998: On the causes of major Baltic inflows- an analysis of long time series. *Continental Shelf Research*, **18**, 67-97.
- SEIFERT, T., KAYSER, B., 1995: A high resolution spherical grid topography of the Baltic Sea. *Meereswissenschaftliche Berichte*, Institut für Ostseeforschung Warnemünde, No.9, 72-87.
- STIGEBRANDT, A., 1985: A model for the seasonal pycnocline in rotating systems with application to the Baltic Proper. *Journal of Physical Oceanography*, **15**, 1392-1404.
- STIGEBRANDT, A., WULFF, F., 1987: A model for the dynamics of nutrients and oxygen in the Baltic proper. *Journal of Marine Research*, **45**, 729-759.
- WALIN, G., 1981: On the deep water flow into the Baltic. *Geophysica*, **17**, 75-93.
- WOLF, G., 1972: Salzwassereinbrüche im Gebiet der westlichen Ostsee. *Beiträge zur Meereskunde*, (H.29), 67-77.
- WYRTKI, K., 1954: Der große Salzeinbruch in die Ostsee im November und Dezember 1951. *Kieler Meeresforschungen*, **10**, 19-25.

Appendix I: Basic Statistics of Time Series

140 m Pos. - NE				140 m Pos. - SW			
Period	A	B	C	A	B	C	D
Time	30.08.97- 27.11.97	28.11.97- 06.05.98	07.05.98- 21.07.98	30.08.97- 27.12.97	28.12.97- 26.05.98	27.05.98- 04.08.98	05.08.98- 08.11.98
N-Days	90	130	106	120	120	100	96
< T> °C	4.91	5.62	6.04	4.94	5.72	5.90	5.83
σ^2 /°C ²	0.003	0.206	0.005	0.001	0.118	0.013	0.008
Min/ °C	4.79	4.92	5.73	4.87	4.90	5.64	5.54
Max/ °C	5.02	7.17	6.22	5.11	6.39	6.13	5.96
Range	0.23	2.25	0.49	0.24	1.49	0.49	0.42

155 m Pos. - NE				155 m Pos. - SW			
Period	A	B	C	A	B	C	D
Time	30.08.97- 27.11.97	28.11.97- 06.05.98	07.05.98- 13.05.98	30.08.97- 27.12.97	28.12.97- 26.05.98	27.05.98- 04.08.98	05.08.98- 08.11.98
N-Days	90	130	7	120	120	100	96
< T> °C	4.98	5.64	(6.04)	5.00	5.74	6.01	5.99
σ^2 /°C ²	0.002	0.214	0.013	0.001	0.084	0.002	0.030
Min/ °C	4.87	4.92	5.90	4.95	5.00	5.82	5.29
Max/ °C	5.07	7.17	6.21	5.06	6.54	6.12	6.11
Range	0.20	2.25	0.31	0.11	1.54	0.30	0.82

170 m Pos. - NE				170 m Pos. - SW			
Period	A	B	C	A	B	C	D
Time	30.08.97- 27.11.97	28.11.97- 06.05.98	07.05.98- 21.07.98	30.08.97- 27.12.97	28.12.97- 26.05.98	27.05.98- 04.08.98	05.08.98- 14.09.98
N-Days	90	130	106	120	120	100	41
< T> °C	5.04	5.67	6.02	5.06	5.85	6.08	6.06
σ^2 /°C ²	0.001	0.148	0.004	0.001	0.071	0.004	0.001
Min/ °C	4.92	4.97	5.82	4.98	5.21	5.89	5.93
Max/ °C	5.11	6.90	6.17	5.11	6.58	6.23	6.14
Range	0.19	1.93	0.35	0.13	1.37	0.34	0.21

Table A.1.

Statistics of temperature records carried out beneath the perennial pycnocline at 140m, 155m, and 170m depth at the NE position and SW position shown in Fig.2. Total series were subdivided by four characteristic situations, which describe the pre-inflow period (A), the inflow period (B), and two post-inflow periods (C, D); all calculations are based on daily averages; the number of days is given by (N); the mean value is < T> with the variance σ^2 ; the difference between maximum; (Max) and minimum (Min) indicates the total range of fluctuation; peak values of each row are given by bold numbers.

170 m Pos. -NE u				170 m Pos. - SW u			
Period	A	B	C	A	B	C	D
Time	30.08.97- 27.11.97	28.11.97- 06.05.98	07.05.98- 21.07.98	30.08.97- 27.12.97	28.12.97- 26.05.98	27.05.98- 04.08.98	05.08.98- 14.09.98
N-Days	90	130	106	120	120	100	41
$\langle u \rangle \cdot 10^2$ (m/s)	-1.9	-3.4	-0.7	0.5	0.9	-1.0	0.9
$\sigma^2 \cdot 10^4$ (m/s) ²	5.81	13.1	4.72	6.71	14.15	12.78	4.62
Min $\cdot 10^2$ (m/s)	-8.0	-13.9	-5.7	-7.4	-12.9	-11.0	-4.9
Max $\cdot 10^2$ (m/s)	5.8	9.9	4.3	6.5	14.7	8.5	5.7
Range $\cdot 10^2$ (m/s)	13.8	23.8	10.0	13.9	27.6	19.5	10.6

170 m Pos. -NE v				170 m Pos. - SW v			
Period	A	B	C	A	B	C	D
Time	30.08.97- 27.11.97	28.11.97- 06.05.98	07.05.98- 21.07.98	30.08.97- 27.12.97	28.12.97- 26.05.98	27.05.98- 04.08.98	05.08.98- 14.09.98
N-Days	90	130	106	120	120	100	41
$\langle v \rangle \cdot 10^2$ (m/s)	2.4	4.6	0.9	-3.0	-4.7	-2.1	-1.6
$\sigma^2 \cdot 10^4$ (m/s) ²	9.46	16.79	6.30	12.53	19.67	8.73	11.05
Min $\cdot 10^2$ (m/s)	-7.5	-5.0	-5.2	-12.6	-24.0	-13.0	-11.4
Max $\cdot 10^2$ (m/s)	11.7	19.1	7.5	3.9	4.5	5.5	3.0
Range $\cdot 10^2$ (m/s)	19.2	24.1	12.7	16.5	28.5	18.5	14.4

170 m Pos. -NE MKE				170 m Pos. - SW MKE			
Period	A	B	C	A	B	C	D
Time	30.08.97- 27.11.97	28.11.97- 06.05.98	07.05.98- 21.07.98	30.08.97- 27.12.97	28.12.97- 26.05.98	27.05.98- 04.08.98	05.08.98- 14.09.98
N-Days	90	130	106	120	120	100	41
$\langle \text{MKE} \rangle \cdot 10^4$ (m/s) ²	12.3	31.3	6.1	14.3	28.4	13.4	9.4
$\sigma^2 \cdot 10^8$ (m/s) ⁴	212.9	1109.1	58.3	237.5	1910.1	356.7	241.4
Min $\cdot 10^4$ (m/s) ²	0.1	0.1	0.1	0.1	0.3	0.1	0.1
Max $\cdot 10^4$ (m/s) ²	76.8	201.0	39.1	79.4	370.9	144.6	77.1
Range $\cdot 10^4$ (m/s) ²	76.7	200.9	39.0	79.3	370.6	144.5	77.0

170 m Pos. -NE EKE				170 m Pos. - SW EKE			
Period	A	B	C	A	B	C	D
Time	30.08.97- 27.11.97	28.11.97- 06.05.98	07.05.98- 21.07.98	30.08.97- 27.12.97	28.12.97- 26.05.98	27.05.98- 04.08.98	05.08.98- 14.09.98
N-Days	90	130	106	120	120	100	41
$\langle \text{EKE} \rangle \cdot 10^4$ (m/s) ²	9.3	21.0	5.0	8.6	13.9	5.8	10.0
$\sigma^2 \cdot 10^8$ (m/s) ⁴	76.4	351.3	22.9	57.0	159.8	55.2	67.0
Min $\cdot 10^4$ (m/s) ²	0.3	0.5	0.2	0.3	0.7	0.3	0.6
Max $\cdot 10^4$ (m/s) ²	48.9	107.6	20.3	37.4	58.9	64.8	37.5
Range $\cdot 10^4$ (m/s) ²	48.6	107.1	20.1	37.1	58.2	64.5	36.9

Table, A.2.

Statistics as in Table A.1. but for the zonal current component (u, positive to east) and the meridional current component (v, positive to north) at 170m depth; all calculations are based on daily averages; the mean kinetic energy per unit mass is $\text{MKE} = (u^2 + v^2)/2$ while the daily eddy kinetic energy is $\text{EKE} = (\sigma_u^2 + \sigma_v^2)/2$.

Appendix II: Baltic Sea Surface Area

For the Baltic Sea, several different figures for its surface area exist in the literature varying between about 380,000 km² and 420,000 km². To be able to refer to a well-defined number, we have recomputed the surface area to be 382,486 km² as described in the following.

i) Geoid model:

In the World Geodetic System 1984 (WGS84, see DMA, 1991) and KUMAR (1993), the Earth ellipsoid model is given by its semi-major axis, $a = 6,378,137.0$ m, and its semi-minor axis, $b = 6,356,752.31425$ m, corresponding to a numerical eccentricity, e , as much as $e^2 = 1 - b^2/a^2 = 6.6943800E-03$. The surface area element on an ellipsoid is

$$dA = r \cos(\phi) d\lambda ds,$$

where λ is longitude, ϕ is latitude, and $r(\phi, \lambda)$ is the local Earth radius, $r^2 = a^2 \cos^2(\phi) + b^2 \sin^2(\phi)$. Here, ds is the meridional distance element given by $ds^2 = [a^2 \sin^2(\phi) + b^2 \cos^2(\phi)] d\phi^2$. Introducing $\tau = \sin(\phi)$, we get

$$dA = a^2 \{ (1 - e^2 \tau^2) [1 - e^2 (1 - \tau^2)] \}^{1/2} d\tau d\lambda.$$

Expanding into powers of eccentricity e up to 4th order and carrying out the integral over τ (i.e. using Stokes' theorem) we obtain

$$dA = ab\tau (1 + e^4 \tau^2 (5 - 3\tau^2) / 30) d\lambda + O(e^6).$$

The integration path is to be extended along closed shoreline polygons $\tau(\lambda)$ of the Baltic sea surface, the islands embedded etc. Between two successive polygon rim points (ϕ_1, λ_1) and (ϕ_2, λ_2) we have assumed a linear relationship between latitude and longitude, $\phi = m\lambda + n$, such that the contour integral for this segment yields the partial area

$$\int_{\lambda_1}^{\lambda_2} dA = \frac{ab(\lambda_2 - \lambda_1)}{(\phi_2 - \phi_1)} * \{ [\cos(\phi_1) - \cos(\phi_2)] (1 + \frac{e^4}{15}) + ([\cos^3(\phi_1) - \cos^3(\phi_2)] \frac{e^4}{90} - [\cos^5(\phi_1) - \cos^5(\phi_2)] \frac{e^4}{50}) \}$$

This expression has been computed and summed up along all relevant Baltic shorelines.

ii) Shoreline Data:

Regionally Accessible Nested Global Shorelines (RANGS, cf. FEISTEL, 1999) have been used for surface area and border length computation, which are organised in closed polygon loops in $1^\circ \times 1^\circ$ cells covering the entire globe. The shoreline points have an absolute accuracy of 500 m and resolve structures in size below 100 m^(*).

iii) Boundary Definition:

Along the greatest part of the Baltic shore, coastal structures (islands, bights, etc) have been accounted for as defined by the RANGS data set, i.e. down to extensions of typically 100 m. In the Belt/Sound region between the Kattegat and the western Baltic Sea, we have defined boundary lines at the narrow gate points as shown in Fig A1:

LiB = Little Belt:	from 09.693250° E, 55.520389° N to 09.696639° E, 55.523722° N
GrB = Great Belt:	from 10.856694° E, 55.294528° N to 11.090806° E, 55.333306° N
Su = Sound:	from 12.624111° E, 56.039194° N to 12.682444° E, 56.045833° N

^(*) Data and additional information are available from the internet homepage:

<http://www.io-warnemuende.de/homepages/rfeistel/>

iv) Error Estimates:

As it follows from the integral formula given above, the terms of order e^4 in eccentricity contribute to about 3 ppm of the Baltic sea surface, that is about 1 km². Higher order terms can be assumed to contribute much less. The sea surface area depends on sea level. Using RANGS, the border line length of the Baltic Sea can be computed as roughly $L = 70,000$ km with the resolution given. For a beach-like shore slope of, say, $dz/dx = 10\%$, a sea level rise of $\Delta z = 0.01$ m causes a progression of sea onto land of $\Delta x = 0.1$ m, and, consequently, an increase in surface area of

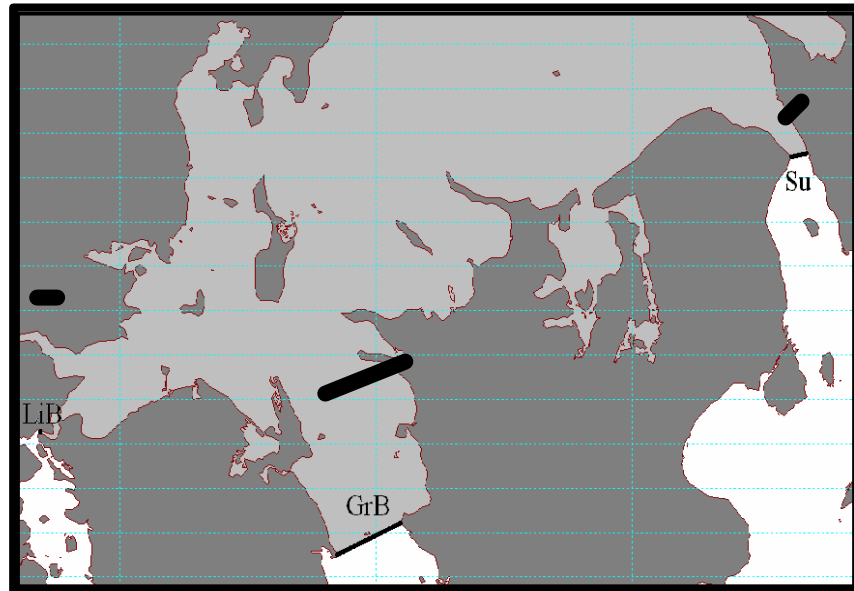


Fig.A1 Selected boundary lines coinciding with narrow gates (bold lines) in transition zones formed by the Little Belt (LiB), the Great Belt (GrB), and the Sound (Su); white areas contribute to the total area $A = 382,486$ km² of the Baltic Sea.

$\Delta A = \Lambda * \Delta x = 7$ km². With a typical sea level variation range of $\Delta z = 0.4$ m at the station Landsort, the related surface area error can be roughly estimated to be of the order of $\Delta A = 300$ km² or 0.1%. The RANGS shoreline data used have typical errors of some $\Delta x = 10$ m and an absolute maximum error of $\Delta x = 500$ m. With the shore length given, the resulting errors are $\Delta A = 700$ km² and $\Delta A = 35,000$ km² respectively. Therefore, the absolute maximum error of the sea surface is about 10%, while the expected error lies in the range between 0.1% and 1%.

References

- DMA, 1991: Department of Defence World Geodetic System 1984: Its definition and relationship with local geodetic systems, DMA TR 8350.2, second edition, 1 September.
- FEISTEL, R., 1999: New shoreline map-drawing data available. EOS, Transactions American Geophysical Union, **80**, Electronic Supplement, June 7, p.249.
- KUMAR, M., 1993: World Geodetic System 1984: A reference frame for global mapping, charting and geodetic applications. Surveying and Land Information Systems, **53**, 53- 56.